BASALT MICROFIBER REINFORCEMENT FOR IMPROVING DESICCATION BEHAVIOR OF CLAY BENTONITE FOR NUCLEAR WASTE DISPOSAL: AN EXPERIMENTAL INVESTIGATION

A Thesis

by

JULIA ANNE GRASLEY

Submitted to the Graduate and Professional School of
Texas A&M University
in partial fulfillment of the requirements for the degree of

MASTER OF SCIENCE

Chair of Committee,	Yong-Rak Kim
Committee Members,	Marcelo Sanchez
	Chandler Benjamin
Head of Department,	Zachary Grasley

December 2022

Major Subject: Civil Engineering

ABSTRACT

Each nuclear power reactor generates 20-30 tons of highly radioactive waste, annually. The preferred long-term solution for highly radioactive waste (HLW) disposal is containment underground in geological repositories. Canisters filed with radioactive waste are placed in tunnels, with one or more engineered barrier materials (EBM) encapsulating them and separating them from the natural rock (i.e., the natural barrier). Bentonite clay is commonly used as an EBM due to its many advantageous properties including low hydraulic permeability, which ensures that only slow diffusion-based transport of radionuclide contaminants is allowed. However, heat-induced desiccation cracking of bentonite clay may increase hydraulic permeability.

An attractive solution may be to reinforce the bentonite clay to prevent desiccation cracking and resulting increase in hydraulic permeability. Fiber reinforcement has commonly been used as a method of improving the properties of various materials and has been effective in reinforcing desiccation cracking. Basalt fiber is a high-density material that has been used to provide physical reinforcement for composite materials (Bella, 2015; Dhand, 2015). There has also been some research on the use of basalt fibers for nuclear waste disposal application. However, there has been limited research on the drying shrinkage and desiccation behavior of basalt microfiber-reinforced bentonite clay.

Basalt microfiber reinforcement was investigated as a method to reduce shrinkage cracking in bentonite clay EBM by generating frictional and tensile resistance within the composite inorganic microfiber reinforced engineered barrier material

(IMEBM). Desiccation behavior was investigated using a free shrinkage and restrained ring test method with digital image correlation (DIC) for data collection and analysis. Free shrinkage was minimally affected by basalt microfiber reinforcement. However, basalt microfiber reinforcement was effective in “bridging” desiccation cracking, preventing complete separation of the material. Therefore, basalt microfiber-reinforced bentonite clay may be an effective solution to limit desiccation cracking in geological repositories and improve nuclear waste management and safety.

DEDICATION

I would like to dedicate this thesis to my dad, Zachary Grasley. I succeeded in never taking one of your courses.

ACKNOWLEDGEMENTS

I would like to thank my committee chair, Dr. Yong-Rak Kim, and my committee members, Dr. Marcelo Sanchez, and Dr. Chandler Benjamin, for their willingness to serve on my committee and provide timely input and feedback for any questions, and for their reviewal of this document.

Thanks also go to my research team members who are working on other aspects of this project, including Abdullah Azzam for his willingness to work alongside me in the laboratory and for his help with DIC setup and analysis, Mohammad Rahmani for his inputs and feedback to improve the testing so that it may be better implemented for modelling, and Ayazhan Bazarbekova for her part in additional testing efforts that are beyond the scope of this document. For the other members of our research team: Shayan Gholami, In Kyu Jeon, Santosh Kommidi, and Dian Setiawan, for any guidance and training, help and comradery in the laboratory, and any ridesharing.

For members of our project team at the University of Nebraska-Lincoln, thanks go to Dr. Jongwan Eun, Dr. Seunghee Kim, Dr. Dongwa Noh, Dr. Yuan Feng, and Ferdinand Calaunan, for their many questions and comments during biweekly project meetings, that have helped to improve and refine all experimentation described in this document. Finally, I would like to acknowledge our collaboration with Dr. Carlos Jove-Colon, Dr. Yifeng Wang, and Amanda Sanchez at Sandia National Laboratories and their feedback in monthly project meetings.

CONTRIBUTORS AND FUNDING SOURCES

Contributors

This work was supervised by a thesis committee consisting of Dr. Yong-Rak Kim [advisor] and Dr. Marcelo Sanchez of the Zachry Department of Civil and Environmental Engineering, and Dr. Chandler Benjamin of the J. Mike Walker ’66 Department of Mechanical Engineering. Digital image correlation setup, calibration, and analysis was aided by research team member: Abdullah Azzam. Modelling efforts for this experimental study will be completed by research team member: Mohammad Rahmani.

All other work conducted for the thesis was completed by the student independently.

Funding Sources

Graduate study was supported by a graduate research assistantship, the Harold J. 'Bill' Haynes '46 Fellowship and the Joseph A. Orr Civil Engineering Graduate Endowed Fellowship, both awarded by the Zachry Department of Civil and Environmental Engineering.

This work was also made possible in part by Nuclear Energy University Programs (NEUP) under Grant ID Number DE-NE0008954. Its contents are solely the responsibility of the author and do not necessarily represent the official views of the Department of Energy (DOE).

NOMENCLATURE

DIC	Digital Image Correlation
EBM	Engineered Barrier Material
EBS	Engineered Barrier System
HLW	High Level Nuclear Waste
IMEBM	Inorganic Microfiber-Reinforced Engineered Barrier Material
SNF	Spent Nuclear Fuel

TABLE OF CONTENTS

Page

LIST OF FIGURES

Page

LIST OF TABLES

Page

CHAPTER I

INTRODUCTION

Nuclear Waste Disposal

Nuclear radiation is used for many applications, mainly as fuel for nuclear power plants and in the production of nuclear weapons for national defense. Each of these applications generates nuclear waste that must be disposed of safely and effectively, to best protect public health and safety. There are three main radiation levels of nuclear waste including high level nuclear waste (HLW), low level nuclear waste, and transuranic. Each nuclear power reactor generates 20-30 tons of highly radioactive waste, annually. High level nuclear waste may remain highly radioactive for a prolonged period, even tens of thousands of years. Thus, HLW, often in the form of spent nuclear fuel (SNF), must be disposed of in a method such that it is isolated and contained long-term.

Geological Repository

Burying the waste deep underground, ensures that any leakage of radionuclides will face sufficiently long transport times, that it may likely decay before reaching the biosphere. Hence, the preferred method of disposal, especially for HLW, is disposal deep underground (typically 250-1000 meters) in a geological repository (Ming, 2022). The geological repository is combined with a redundant multi-barrier approach where one or more engineered barrier materials (EBM) will encapsulate and separate the

nuclear waste, which is contained in a metal canister or container, from the natural rock formation (i.e., the natural or geological barrier).

Bentonite as an Engineered Barrier Material

Bentonite clay is a common choice for an engineered barrier material due to its many advantageous properties including:

- Availability as a natural material
- Low:
    - Cost
    - Hydraulic permeability in a saturated state
- High:
    - Long-term stability
    - Physio-chemical compatibility with both natural rock and nuclear waste
    - Thermal resistance
    - Radionuclide retardation capacity
    - Swelling pressure
- And self-healing capability.

Bentonite clay as an EBM can restrict the mobility of radionuclide contaminants, due to its low hydraulic permeability. This property ensures that slow diffusion will be the dominant transport mechanism of contaminants (Leupin, 2013). In addition, bentonite's high swelling pressure can function as a self-healing capability to seal any gaps formed in the barrier.

There has been notable research into the design of engineered barrier systems in geological repositories, with bentonite clay as the engineered barrier material. Europe is at the forefront of nuclear waste research, testing, and construction of waste disposal systems. For example, the Swedish company SKB's final disposal method termed KBS-3 is based on three protective barriers:

1. copper canisters with nodular cast iron inserts to withstand corrosion and mechanical forces from underground rock movement,
2. bentonite clay as the buffer material to protect the canister from corrosion and movements, absorb water and swell to fill the space around the canister and any cracks in the rocks, prevent water from entering the canister, and prevent the transport of any contaminants into the rock, and
3. bedrock to isolate the waste from human interaction and the natural environment, provide a stable chemical environment, and protect the canister from any events or disasters that may occur at the ground level.

Other European companies such as POSIVA in Finland, ANDRA in France, and DBE in Germany, are also based on a similar design concept (Akesson et al., 2009). Testing of bentonite clay for nuclear waste disposal has included simplified laboratory testing to study specific properties such as swelling potential, mechanical properties, etc., complex laboratory testing to replicate the complex thermo-hydro-mechanical conditions in a geological repository, and in-situ testing. Perhaps most notable is the FEBEX (Full-Scale Engineered Barrier EXperiment), which is based on the Spanish concept for disposal of radioactive waste in crystallin rocks. The FEBEX project

included complex laboratory testing with experimental results up to eight years, and two large scale tests: an in-situ test at the Grimsel underground laboratory in Switzerland, and a mock test at CIE-MAT (Research Center for Energy, Environment, and Technology) in Madrid, Spain (Alonso et al., 2009; Alcoverra et al, 2021; Gens et al, 2008; Sampler & Zheng, 2008).

The Desiccation Cracking Problem

Heat that is generated due to radioactive decay of the nuclear waste in the initial stages will lead to drying and contraction of the bentonite clay near the nuclear waste container. Clayey soils, such as bentonite clay, are prone to desiccation cracking. Some cracking may be self-healed when the ground water from the natural rock reaches the bentonite near the canister, allowing it to swell and seal any cracks that formed. However, in the meantime, heat-induced desiccation cracking may drastically increase hydraulic permeability (Gao, 2011; Mohammad, 2020)

The complex thermo-hydromechanical interaction of radioactive decay-generated heat release from the canister, groundwater inflow from the natural rock barrier, and the restrained conditions underground can make it challenging to predict and control the extent of desiccation cracking and the resulting increase in hydraulic permeability. If large cracks or crack networks are allowed to form, they can act as pathways for the transport of contaminants through the barrier.

It is necessary to devise a research solution to prevent, restrain, or reduce the damage and extent of desiccation cracking in bentonite clay EBM, to prevent any transport of toxic contaminants through nuclear waste barriers, so that nuclear waste management practices best secure public health and safety.

Fiber Reinforcement

Traditional methods of improving the mechanical properties of soil include chemical admixtures or soil curing. Fiber reinforcement for soils is a physical reinforcement technique where fiber filaments are uniformly dispersed into the soil to improve the mechanical properties of the soil-fiber composite. Fiber reinforcement has been used to improve the properties of various composite materials. Studies have been conducted on the effectiveness of fiber reinforcement in providing physical reinforcement to restrain desiccation cracking and improve the tensile strength of materials (Abdi et al., 2008; Dong, 2021; Kouta, 2020). Fibers that have been used include various types of both natural and synthetic fibers. Previous research into synthetic fiber usage in clayey soils includes mainly polypropylene fiber (Cui, 2012; Cyrus, 2008; Soujanya, 2017), as well as glass and carbon fiber.

Basalt Fiber Reinforcement

Basalt fiber is a type of inorganic synthetic fiber, with an elastic modulus and tensile strength significantly higher than conventional polypropylene fiber (Czigany, 2019). Basalt has been used to provide physical reinforcement for various composite materials. There has been some research conducted on the use of basalt fiber for

radioactive waste disposal application. Notably, Biland et al. (2019) showed an increase in nuclear radiation shielding of up to 13.0 % from the addition of basalt-boron fiber to concrete specimens, and Azhari and Isfahani (2020) showed basalt fiber reinforcement to be effective in improving the nuclear radiation shielding performance of bentonite clay.

Regarding improvement of the mechanical properties of composites, particularly for controlling desiccation cracking, more research has been conducted on the addition of basalt fibers to concrete. Chen et al. (2021) showed that with increasing amounts of short-cut basalt fiber, the early desiccation cracking behavior of concrete will improve, with reduction in the width, length, and depth of cracking. Branston et al. (2016) showed that basalt fiber prevented early shrinkage cracking of concrete by reducing the magnitude of free shrinkage and restricting the growth of cracks that occurred.

Conclusions

Bentonite clay is commonly used as an engineered barrier material due to its many advantageous properties including low hydraulic permeability, which ensures that only slow diffusion-based transport of radionuclide contaminants is allowed. However, heat-induced desiccation cracking of bentonite clay may increase hydraulic permeability. An attractive solution is to reinforce the bentonite clay to prevent desiccation cracking and resulting increase in hydraulic permeability. Fiber reinforcement has commonly been used as a method of improving the properties of various materials and has been shown effective in preventing desiccation cracking. Basalt fiber is a high-density material that has been used to provide physical reinforcement for various composite

materials. There has also been some research on the use of basalt fibers for nuclear waste disposal application. However, there has been limited research on the drying shrinkage and desiccation behavior of basalt microfiber reinforced bentonite clay for nuclear waste disposal application.

Research is needed on the effect of basalt fiber reinforcement on the desiccation behavior of clayey soils, including bentonite clay. To accomplish this goal a Restrained Ring with digital image correlation test method was applied to determine the effect of basalt microfiber reinforcement on desiccation cracking. A free shrinkage test was also carried out. It was determined that basalt microfiber reinforcement minimally reduces free shrinkage rate and greatly reduces desiccation cracking severity. Thus, basalt microfiber reinforcement may be an effective solution to improve desiccation behavior in bentonite clay, for the safe disposal of nuclear waste.

CHAPTER II

EXPERIMENTAL METHOD

Desiccation Behavior

It is common knowledge that desiccation cracking in clayey soils is formed when the tensile stress caused by suction exceeds the tensile strength of the material. When a fully saturated homogeneous clayey soil is subjected to drying, the superficial water evaporates first. With the evaporation of additional water, an air-water meniscus is formed between the clay particles, causing the capillary suction between the particles to increase. Thus, the soil shrinks and consolidates as the capillary meniscuses increase, and the clay particles move closer together (Cheng, 2021).

A tensile stress field is developed due to the stress of capillary suction. If the soil shrinkage is unrestrained and uniform then the soil undergoes free shrinkage, without the initiation of any cracks. At the microscopic scale, the clay particles are rearranged closer to each other and at the macroscopic scale volumetric shrinkage occurs. The extent of shrinkage increases with increasing soil plasticity. Bentonite, which is composed of the clay mineral montmorillonite, is a highly plastic clay. Thus, it absorbs more water, and undergoes significant volumetric shrinkage during drying. This also increases the severity of desiccation cracking (Gao, 2020).

Any external or internal restraint can lead to the buildup of tensile stresses exceeding the tensile strength of the material. Once the tensile strength is exceeded crack initiation occurs. Examples of external restraints include physical boundaries restraining the movement of the soil, or friction and adhesion from rough boundary surfaces

(Bouchemella, 2019). Internal restraints arise from nonuniformities. These may be either non-uniform drying, or any pre-existing defects or inhomogeneities, which act as stress concentration points where cracking will initiate.

Restrained Ring with DIC Test Method

Digital Image Correlation

Digital image correlation (DIC) is a precise optical non-contact technique used to measure displacements and enable the calculation of strains by identifying the two-dimensional or three-dimensional transformations of many specific points between reference and deformed digital images (Barton, 1996). DIC is an effective method for tracking desiccation shrinkage and cracking displacements and can be used to determine the evolution of strains that cannot be analyzed through other visual imaging software techniques (Hild, 2006). DIC analysis includes capturing images throughout the stages of crack initiation and development, comparing images taken during crack progression to an initial reference image (i.e., taken before any damage occurs) to determine the evolution of displacements and strains, and analysis of many parameters to characterize cracking, including analysis of the displacement and strains around identified crack tips (Hirose, 2018).

Restrained Ring Test Method

A restrained ring test method has been commonly used and standardized for the determination of the tensile properties of cement concrete (Braudeau et al., 2009; Brescia-Norambuena et al., 2020; Bulut, 2020; D'Ambrosia, 2011; Dong, 2018). More

recently this test method has been applied for soil experimentation. Kodikara et al. (2015) used the restrained ring test with DIC to investigate the tensile strength of desiccating clay soils by isolating the initiation of a single crack, to model mode I cracking, and obtain fracture properties of the propagating crack (Amarisiri et al., 2014), and to determine the J integral, an important parameter in elasto-plastic fracture mechanics (Costa et al., 2012; Costa, 2009; Shannon, 2013). Chen et al. (2020) used the restrained ring test method to determine the evolution of tensile stress with suction.

Most notably, Eid et al. (2021) used the restrained ring with DIC test method to determine the effect of oriented flax fiber reinforcement in kaolin clay. This study is perhaps most like the work described herein, with different material types, oriented instead of random fiber distribution, and a different research application. They were able to obtain the evolution of the radial and circumferential (i.e., hoop) strains at the major crack tip and compare between plain and fiber reinforced specimens. It was found that the addition of flax fibers had no significant effect on global shrinkage but a major influence on crack ratio and the amount of crack opening. From the strain analysis, it was determined that the addition of flax fibers significantly reduces the evolution of the major principal strain leading to crack initiation.

The restrained ring test method generally consists of preparing a ring-shaped soil specimen with a rigid ring placed in the center to provide external restraint. The specimen is allowed to lose moisture and shrink towards the inner restraining ring in its center, which will restrict further shrinkage. This leads to a buildup of compressive radial stresses in the soil and in-turn tensile stresses develop in the hoop direction.

In the absence of any internal defects leading to stress concentrations, the major tensile stresses develop at the soil-ring interface, causing cracking to initiate from the ring and propagate radially to the outer circumference of the specimen. Thus, specimens should be prepared as homogeneous as possible, and non-uniform drying or non-uniform moisture content distribution should be avoided. Generally compacted, consolidated, or specimens in a slurry state are chosen. If drying is allowed only from the top surface, samples should be kept relatively thin to avoid any large moisture gradients from forming.

In addition, the soil boundary surfaces should be sufficiently smooth to avoid any shear stresses from developing or any frictional resistance. If the soil-ring interface is smooth, the radial and hoop stresses can be considered as the principal stresses. Any crack that initiates from the major tensile hoop stress will propagate radially until the edge of the specimen is reached or hoop stresses are too small for cracking to propagate further.

Sample Fabrication

Materials

Sodium bentonite reinforced with inorganic basalt microfibers was used as the Inorganic Microfiber Reinforced Engineered Barrier Material (IMEBM) in this research. The relevant properties of the bentonite, obtained by research project collaborators at The University of Lincoln-Nebraska, are summarized in Table 1.

Table 1. Properties of sodium bentonite clay

Liquid Limit (%)	Plastic Limit (%)	Plasticity Index (%)	Optimum Water Content (%)	Maximum Dry Unit Weight (kN/m^3)
410-500	85-100	310-400	35	12.5

The inorganic basalt fibers were obtained from an online supplier as a spool of thread, which was cut into small fibers of 12.7 mm (0.5 in) in length. The fibers have constant diameter of 0.035 to 0.05 mm and tensile strength of 3000 to 4800 MPa. The microfibers were randomly oriented and fiber percentages of 0.0, 0.5, 1.0, 1.5 % by weight were used for both free shrinkage and restrained ring testing.

Free Shrinkage Specimens

Granular bentonite clay was oven-dried overnight for 24 hours at 110 C, crushed with a soil grinder in the laboratory, and sieved. Bentonite powder passing the 75 μm. (No. 200) sieve was used for all sample fabrication, due to the high sample uniformity that could be achieved with fine bentonite powder. Figure 1 shows the bentonite clay in a granular state and after grinding.

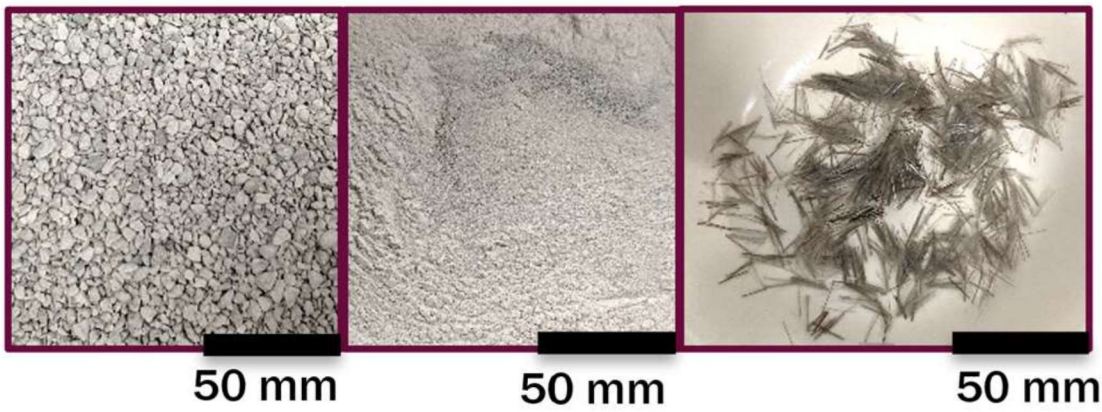

Figure 1. (a) Granular bentonite, (b) ground bentonite powder, and (c) basalt microfiber reinforcement cut to 12.7 mm (1/2 in) length

The dry ingredients (i.e., oven-dried powdered bentonite with or without basalt microfibers) were first mixed and de-clumped. To prevent any re-clumping of the fibers, water was added and stirred into the dry mixture in small increments until it reached the liquid limit. The mixture was hand-compacted into a 100 mm (4 in) oedometer ring with 10 mm thickness. Before molding, the oedometer ring was coated with a thin layer of lubrication jelly. This prevented any cohesion of the bentonite clay to the ring surface, which could cause damage to the sample during demolding. Molded samples were placed in an oedometer cell. A loading pressure of 90 kPa (13 psi) was applied to the top surface of the specimens until constant deformation was observed for an hour, for a maximum duration of 2 hours. During loading and unloading, the specimens were inundated with water. Note that this step was only performed to improve sample uniformity and consistency (e.g., solidify the sample enough for demolding). After removal from the oedometer cell, specimens were extruded from the oedometer ring,

placed on a smooth lubricated plexiglass sheet, and speckled with a fine black carbon powder on their top surface.

Restrained Ring Specimens

For the restrained ring test, an inner restraining ring of 30 mm diameter was punched into the center of the disk specimens and the excess material inside the inner restraining ring was removed. The insertion method ensured good contact between the bentonite sample and the restraining ring. The inner restraining ring was also coated in lubrication jelly before insertion to minimize any bonding of the samples with the ring and any shear effects at the soil-ring interface. Figure 2 summarizes the sample fabrication. Note that all other sample fabrication steps were the same for both free shrinkage and restrained ring specimens.

Figure 2. Sample preparation for free shrinkage and restrained shrinkage specimens

Test Setup

Digital image correlation (DIC) was used to capture the displacement field, and the evolution and propagation of cracks in each specimen when subjected to desiccation. Two DIC cameras obtained from Correlated Solutions with 1920 x 1200 pixels were set

up above the samples to record any three-dimensional displacements and two CSI cool LED lights were used to provide adequate illumination conditions. To track the displacement of the specimens during desiccation, the top surface of the specimens were sprinkled with an exceptionally fine black carbon powder.

The post processing of images was conducted using VIC-3D software designed by Correlated Solution to analyze the effect of fiber on developed strain field, cracking properties, and shrinkage due to moisture loss. Before testing DIC calibration was conducted using a dot grid pattern by taking 20-25 calibration images of the grid at different orientations. This determined each camera's intrinsic parameter (i.e., scale parameter, image skew, image center, and distortion parameter) as well as the position of the target sample. Sample images were taken in intervals of every 1-5 minutes (i.e., depending on the rate of specimen shrinkage and crack initiation) until crack initiation and completion. The subset size used depends on the quality of speckling. A 47 x 47 pixels subset size was observed to be reasonable with a 7 pixels central distance between subsets.

Free and restrained shrinkage tests were conducted for both plain and microfiber-reinforced specimens. The restrained shrinkage tests were implemented using the restrained ring test method.

During testing, specimens were placed on a smooth plexiglass sheet coated with a thin layer of lubrication jelly to minimize any frictional restraint along the bottom of the specimens and prevent moisture loss from the bottom surface of the sample. Because

the sides of the specimens were also coated in a thin layer of lubrication jelly from the oedometer ring, only top surface drying (i.e., one-dimensional drying) was allowed.

The specimen thickness was kept purposely small compared to the diameter, to prevent any large moisture gradients during drying. A laboratory scale with an accuracy of 0.001 g was used to record the moisture loss during the drying process. All desiccation testing was conducted in the laboratory conditions of 22 C and 40 % relative humidity. The complete test setup is shown in Figure 3.

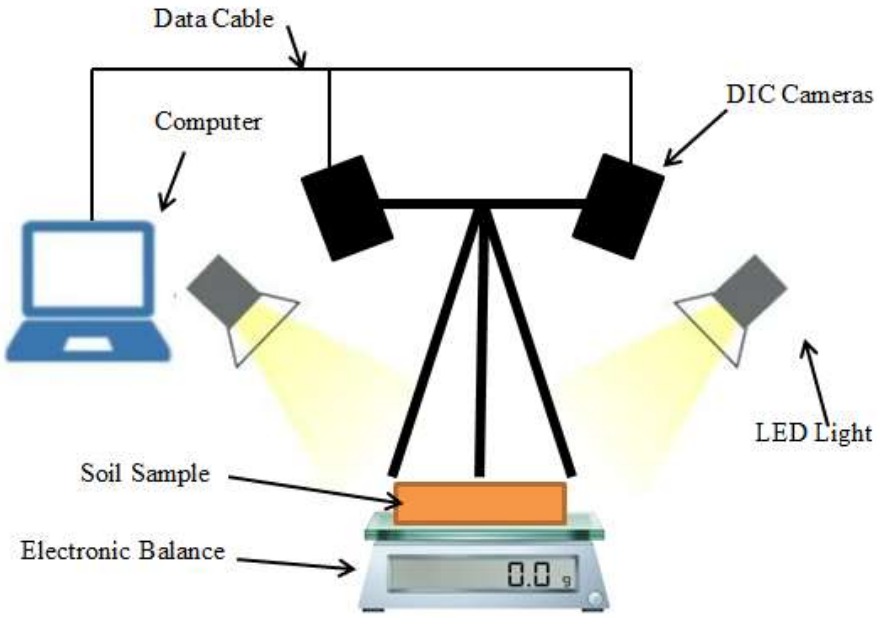

Figure 3. Simplified test setup for free shrinkage and restrained shrinkage testing

Feasibility Testing

Preliminary work was conducted to determine the feasibility of the testing and the feasibility of the sample fabrication, primarily the homogeneity of fiber-mixed samples and the DIC speckling method to be implemented.

Fiber Mixing

Fiber mixing using different fiber percentages and mixing methods was conducted to determine the optimum method to achieve maximum sample homogeneity, specifically with the most uniform fiber distribution. Maximum sample uniformity was obtained when preparing specimens at high water contents, due to a fiber-clumping effect that was observed at low water contents. It was also found that sample homogeneity was improved by grinding the granular bentonite to a fine powder, separating the microfibers before mixing, and mixing the dry ingredients (i.e., powdered bentonite and fiber) before adding the mixing water in small increments. Thus, for the sample fabrication, oven-dried powdered bentonite and separated basalt microfibers were dry-mixed, and then water was added in small increments until the mixture reached the liquid limit for bentonite clay (410-500 %). The resulting fiber distribution after following the fiber mixing method is shown in **Figure 4**.

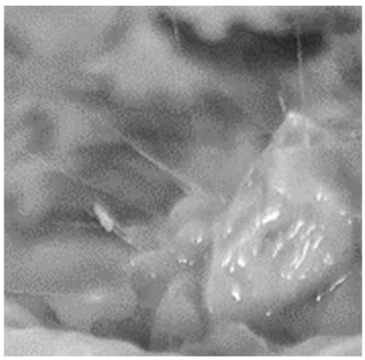

Figure 4. Close-up of fiber distribution after mixing

Speckling Testing

To determine the best speckling method for tracking the movement of bentonite particles during testing with the digital image correlation (DIC) cameras, the optimum speckling method was determined. Generally, DIC data quality increases with increasing color-contrast on the specimen surface. The traditional method for achieving high color-contrast on a specimen surface, is to paint the specimen with a white spray paint and then speckle black spray paint on top. However, it was hypothesized that using any paint will greatly impede surface drying. Speckling a fine black carbon powder over the surface of the sample was determined to be the best method of speckling without preventing substantial moisture loss from the surface of the sample. Figure 5 compares the shrinkage of specimens with spray paint versus carbon powder speckling, showing that paint significantly impeded the drying compared to the powder speckling.

(a) (b)

Figure 5. Comparison of (a) spray paint, versus, (b) carbon powder speckling's effect on the amount of drying shrinkage with the initial size of the specimens marked

To obtain the best size and distribution of speckles, a speckling device was constructed consisting of a series of aluminum foil meshes. Figure 6 shows a scheme of the speckling device used.

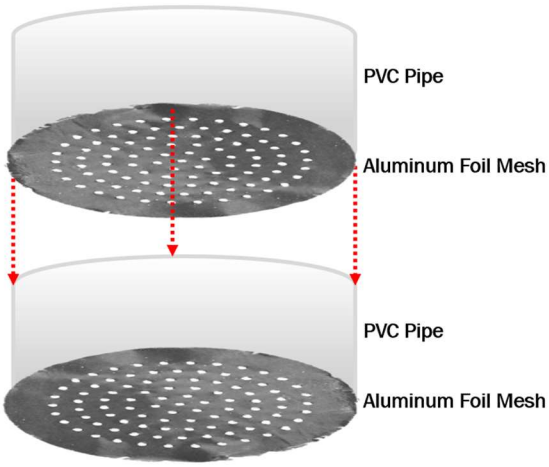

Figure 6. Extruded view of speckling device constructed from a series of hollow PVC pipe sections and aluminum foil mesh

The small mesh hole size controlled the rate of carbon powder falling on the samples and the resulting size of the speckles. Thus, it allowed small speckles to be applied at a slow rate, so that adequate time could be taken to obtain a good distribution of speckles over the whole sample surface. Forcing the powder through multiple meshes also controlled the rate of speckle application. The device was operated by shaking it back and forth over the sample surface, like manually shaking a sieve.

Petri Disk Testing

Preliminary testing was conducted with specimens prepared using the optimum fiber-mixing and speckling methods that were determined. The specimens were hand-mixed and hand-compacted into a petri-dish, and then dried at room temperature and humidity. Both free shrinkage and desiccation cracking deformation and strains were recorded and determined, respectively. Desiccation cracking initiated near the outer edge of the specimens because of the restrained condition caused by bonding of the specimen with the sides of the petri-dish container.

Free shrinkage specimens were prepared by coating the sides and bottom of the petri-dish container in Vaseline lubrication to prevent any bonding effect. Free shrinkage specimens shrank towards the center of the sample, away from the sides of the container.

The evolution of cracking for a restrained petri-dish sample is shown in Figure 7.

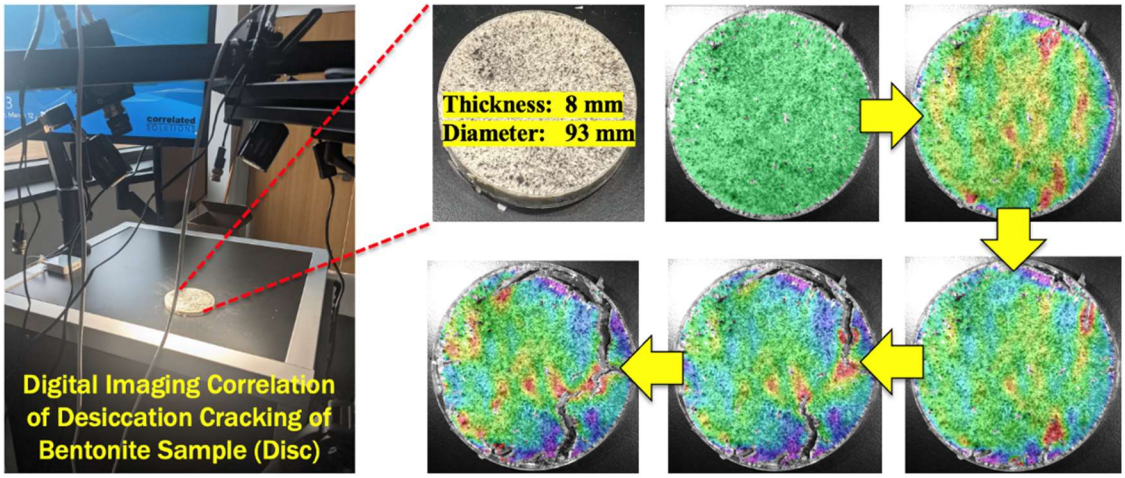

Figure 7. Evolution of cracking in restrained petri-dish testing

Conclusions

Desiccation cracking in bentonite clay occurs when any external or internal restraint leads to the buildup of tensile stresses exceeding the tensile strength of the material. A Restrained Ring test method, with digital image correlation (DIC) for data collection and analysis was applied to evaluate desiccation behavior. Feasibility studies investigated both the sample fabrication and test setup, which were described in detail.

CHAPTER III

FREE SHRINKAGE BEHAVIOR

Introduction

Free shrinkage of disk-shaped bentonite clay specimens with 0.0, 0.5, 1.0, and 1.5% basalt microfiber by weight was recorded over a testing period of 3-5 days. Only one-dimensional top-surface drying was allowed. During testing the specimens shrank radially towards their center. Significant reduction in specimen size and weight was recorded during testing. There was minimal decrease in specimen thickness compared to the significant reduction in specimen diameter. It can also be noted that the free shrinkage specimens did not experience cracking during testing. Thus, the Vaseline lubrication applied to the sides and bottom of specimens, was effective in preventing frictional restraint during testing. Similarly, the sample fabrication method was successful in preventing sample irregularities or defects that could cause internal cracking and unexpected results during free shrinkage testing. Moisture loss of all specimens was measured indirectly by measuring the weight change of specimens during desiccation. Additionally, the evolution of the radial, circumferential, and vertical displacement and strain fields was successfully determined by the digital image correlation (DIC) method. Note that the results shown in each figure throughout this chapter represent the average of the results from three or more sample replicates for each basalt microfiber content, except for the radial and hoop strain fields, where a representative sample for each fiber content was chosen.

Results and Discussion

Diameter Change

DIC was used to track the change in specimen diameter during desiccation testing. The change in diameter was determined by observing the change in distance between two speckle points on opposite edges of each replicate's outer diameter during testing. For each replicate and each timestep the diameter was measured at four different angles and the average was taken to represent the diameter change of free shrinkage disk specimens during testing. It can be noted from the diameter change in Figure 8 that the free shrinkage behavior or trend observed was similar between plain bentonite and basalt microfiber-reinforced specimens. However, overall, the rate of free shrinkage was minimally reduced by basalt microfiber inclusion. This resulted in slightly lower free shrinkage extent (i.e., at each timestep and by the end of testing) for 1.0 and 1.5 % fiber.

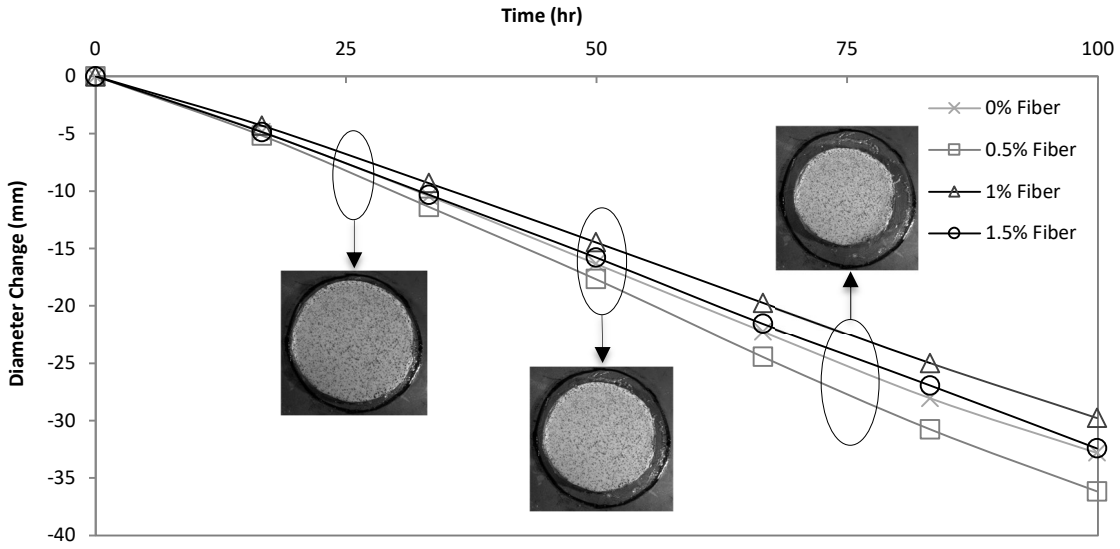

Figure 8. Diameter change of free shrinkage disk specimens

Moisture Loss

Specimen weight was recorded during testing and each replicate was oven-dried for 24 hours after testing to back-calculate the moisture content change during testing. The same conclusions that were deduced from the average change in shrinkage can also be inferred from comparing the moisture loss profile trends between different fiber contents. Namely, that the free shrinkage behavior or trend is similar between plain bentonite clay and microfiber-reinforced bentonite, while the rate and total extent of free shrinkage was minimally impacted by microfiber reinforcement. Weight change and moisture loss profiles for each fiber content are shown in Figure 9 and Figure 10, respectively.

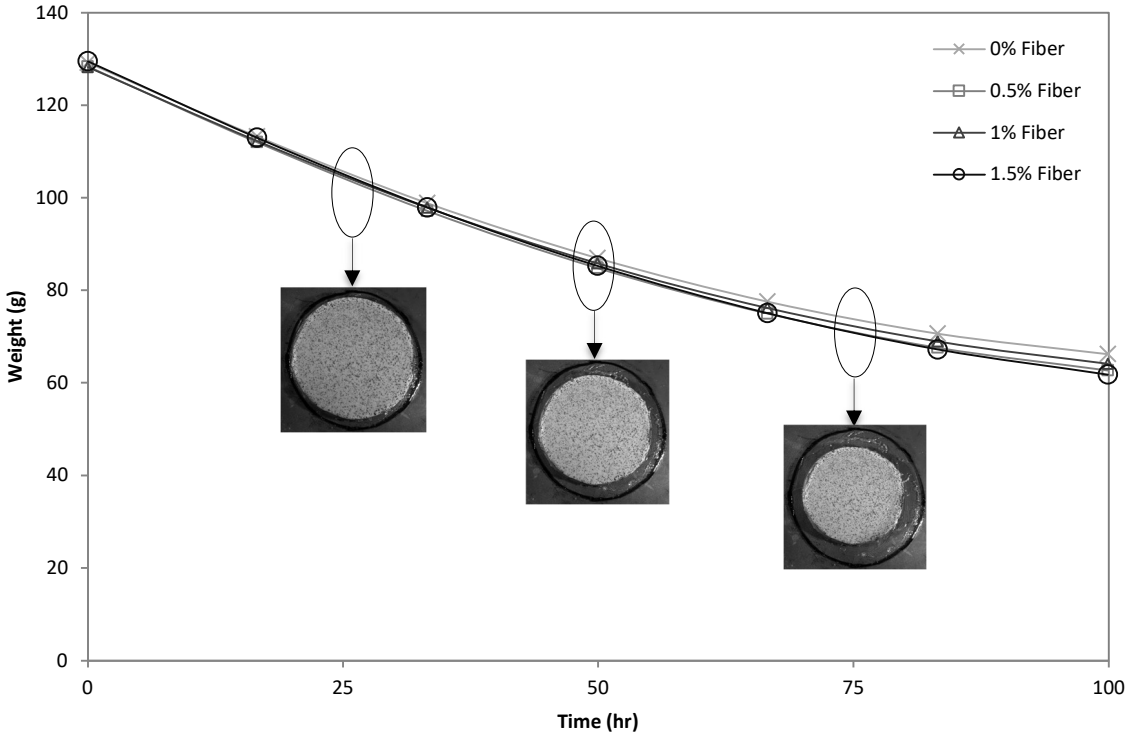

Figure 9. Weight change of free shrinkage disk specimens

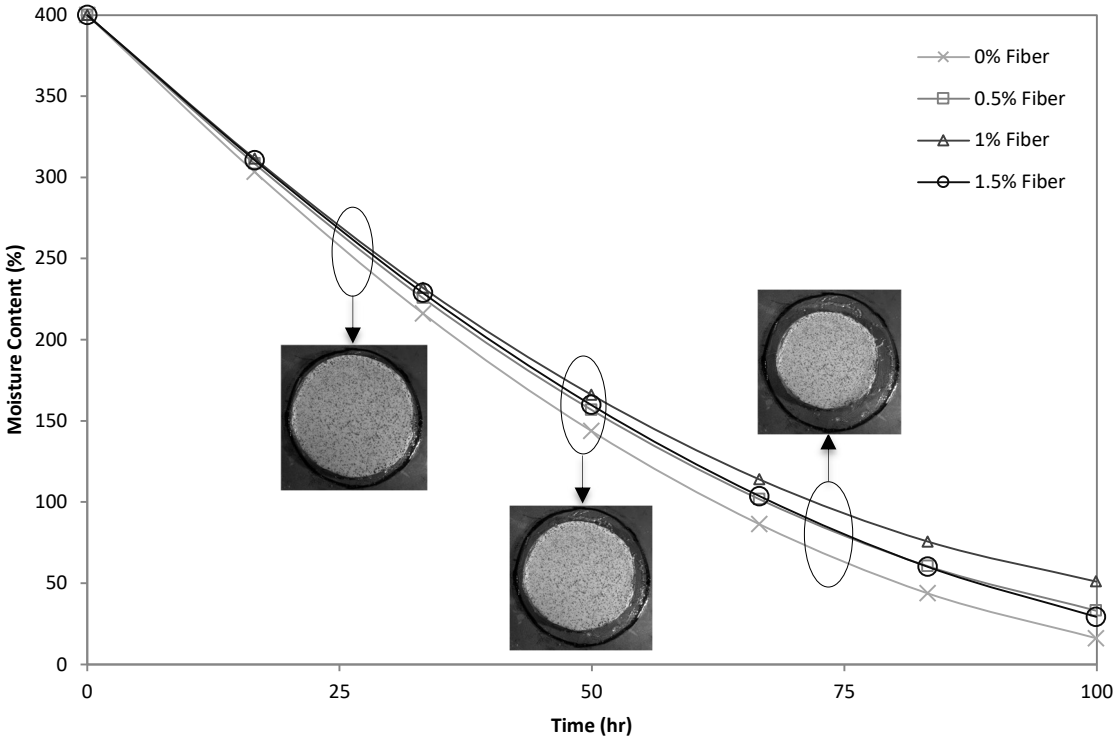

Figure 10. Moisture loss profiles of free shrinkage disk specimens

Evolution of Radial and Hoop Strains

The evolution of radial strains and hoop strains are visualized in Figure 18 and Figure 19 respectively. Each strain field is shown at three different time steps, namely after 0, 50 and 100 hours of desiccation at the laboratory-controlled condition. It is to be noted that the DIC VIC-3D software has the capability to provide Lagrangian strains in the principal axes. Strain conversion from cartesian coordinates to polar coordinates was conducted by applying a conversion function on the data as shown in Equation 1 and Equation 2.

$$\epsilon_{rr} = \epsilon_{xx}\, cos^2\, \theta + \epsilon_{yy}\, sin^2\, \theta + \epsilon_{xy}\, sin\, 2\theta \qquad \textbf{Equation 1.}$$

$$\epsilon_{\theta\theta} = \epsilon_{xx} \sin^2 \theta + \epsilon_{yy} \cos^2 \theta - \epsilon_{xy} \sin 2\theta \qquad \textbf{Equation 2.}$$

Where:

ϵ_{rr}& $\epsilon_{\theta\theta}$ are the radial and hoop strains, respectively,

$\epsilon_{xx}, \epsilon_{yy}$ & ϵ_{xy} are the strains in cartesian coordinates,

And,

θ is the angle measured from the disc center to the point of interest, measured counterclockwise.

From visual examination of the pictures in Figure 18 and Figure 19 for radial and circumferential (i.e., hoop) strain, it is also apparent that free shrinkage behavior, trend, and extent was similar between the different microfiber contents. However, fiber-reinforced bentonite samples showed lower radial and hoop strains compared to plain bentonite samples. The magnitude of radial and hoop strains developed during testing were also quantified and compared between fiber contents by measuring the radial and hoop strains around the circumference of a representative sample from each fiber content. Figure 11 shows the location of radial and hoop strain measurements on a representative sample.

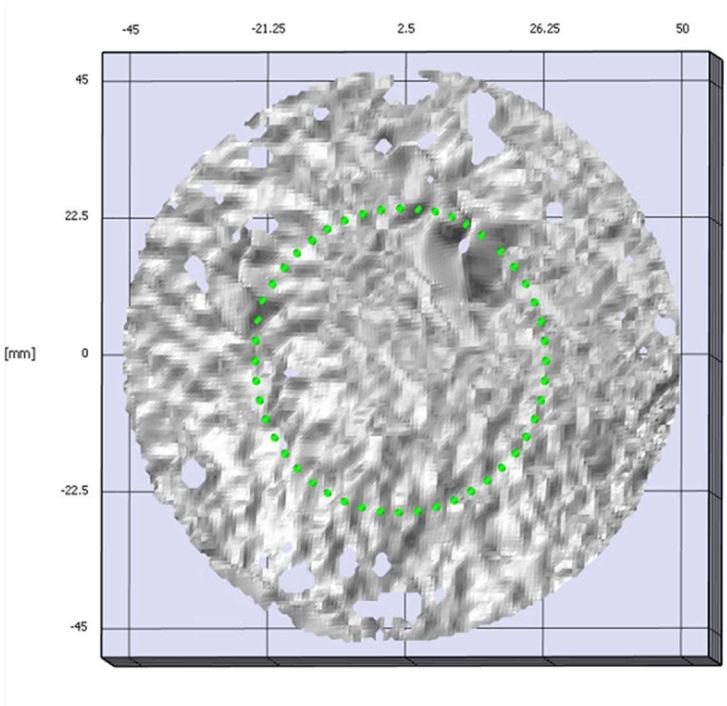

Figure 11. Circle with points marked showing the location of radial and hoop strain measurements around the circumference of a sample

Measurements of radial and hoop strains were taken at 50 and 100 hours. The variation of radial and hoop strains with angle (θ) around each sample circumference are shown after 50 hours of testing in Figure 12 and Figure 13, and after 100 hours of testing in Figure 14 and Figure 15.

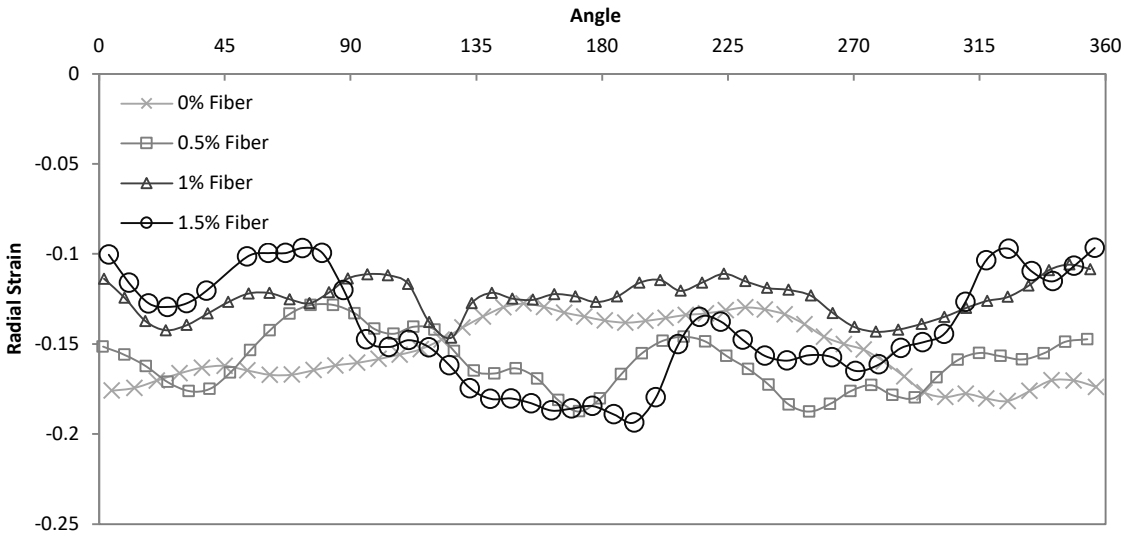

Figure 12. Variation of radial strain with angle (θ) around the specimen circumference after 50 hours of testing

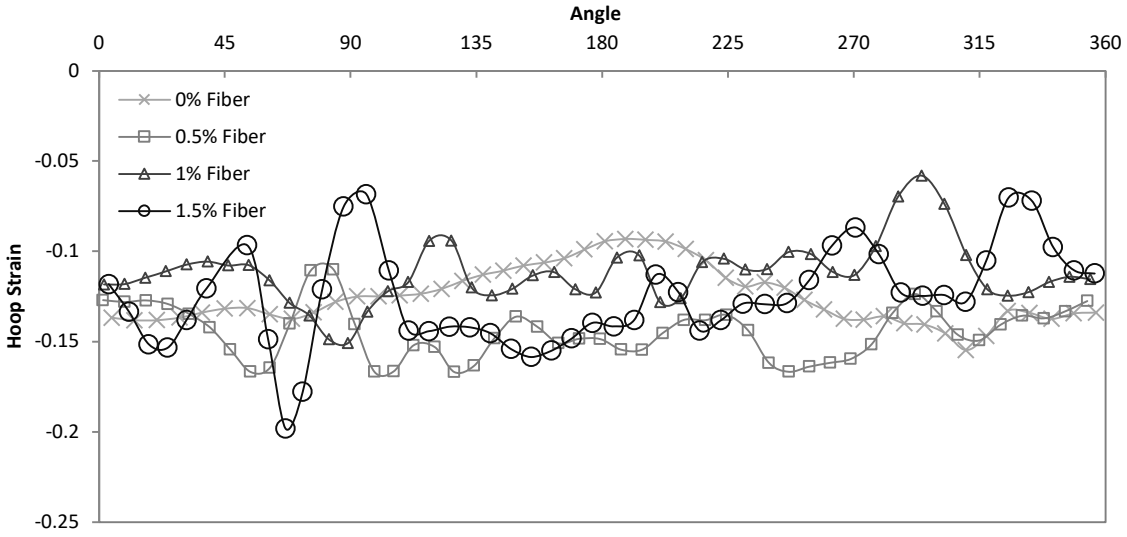

Figure 13. Variation of hoop strain with angle (θ) around the specimen circumference after 50 hours of testing

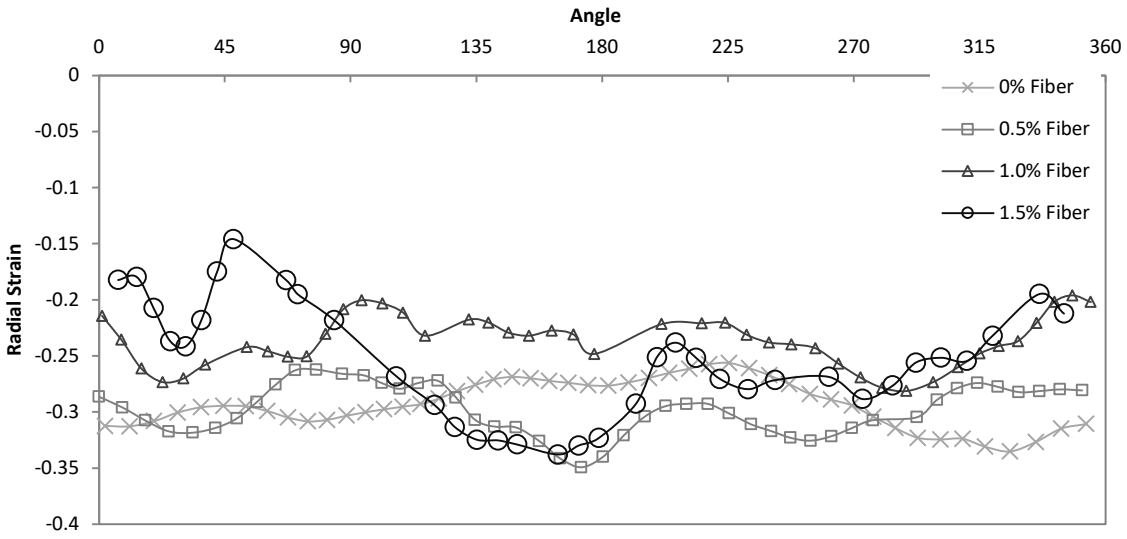

Figure 14. Variation of radial strain with angle (θ) around the specimen circumference after 100 hours of testing

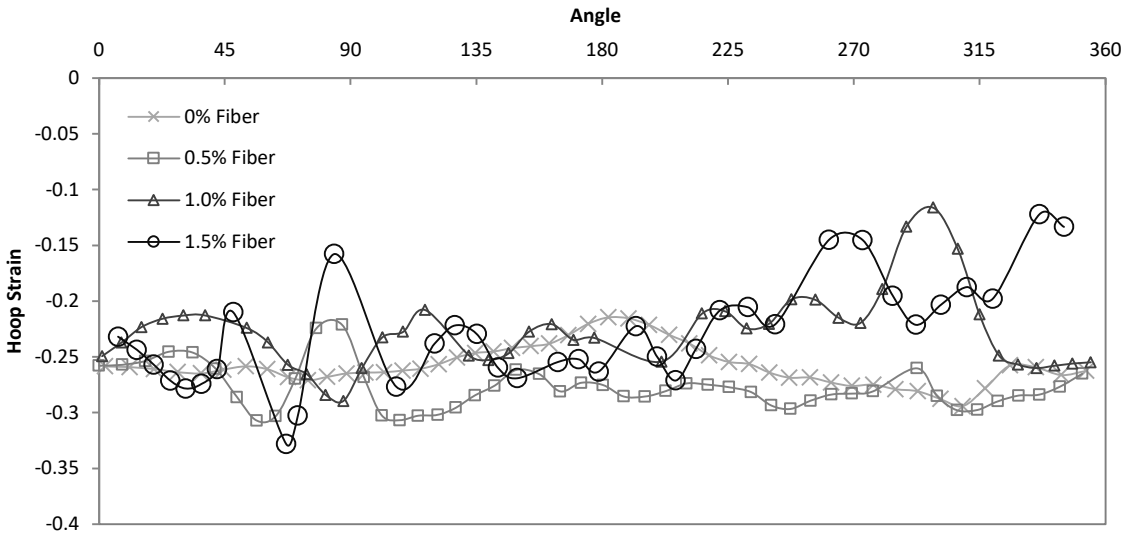

Figure 15. Variation of hoop strain with angle (θ) around the specimen circumference after 100 hours of testing

Average radial and hoop strain values (i.e., the average of all the data points taken in Figure 11) were calculated to numerically compare the magnitude of radial and

hoop strain developed for each fiber content. The average radial and hoop strain magnitudes are shown in Figure 16 and Figure 17, for 50 and 100 hours, respectively.

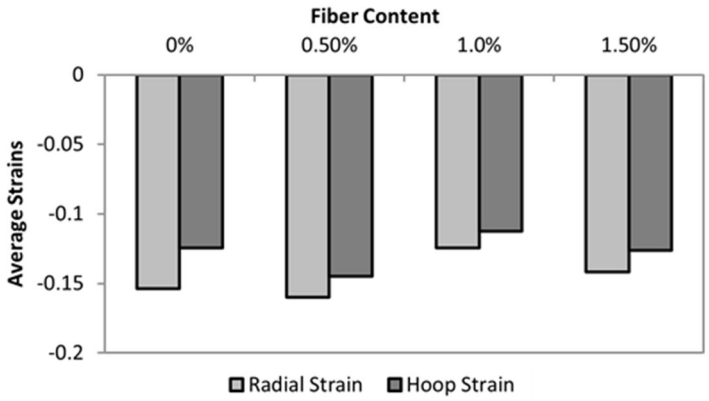

Figure 16. Average radial and hoop strains after 50 hours of testing

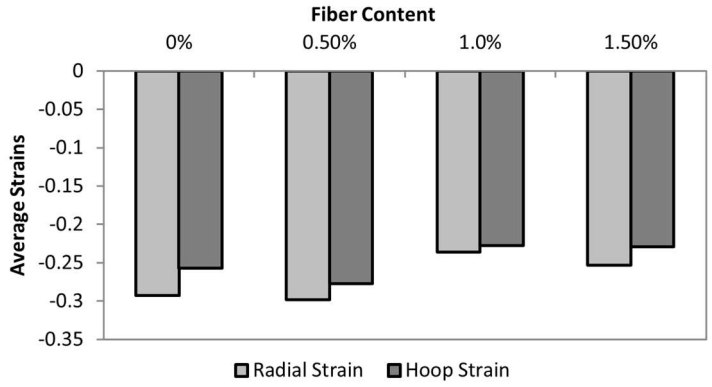

Figure 17. Average radial and hoop strains after 100 hours of testing

The average radial and hoop strains were minimally reduced for 1.0 and 1.5 % fiber, with the lowest radial and hoop strain values occurring at 1.0 % fiber content, after both 50 and 100 hours of testing. This validates the conclusion that free shrinkage rate and extent were minimally reduced by basalt microfiber inclusion. Overall, 1.0 % microfiber-reinforced bentonite showed the lowest shrinkage extent according to all free shrinkage measurements, including lowest rate of diameter decrease, lowest rate of

moisture loss, and lowest radial and hoop strains during testing. Also, note that large strains were recorded during testing, therefore small strain measures such as the infinitesimal strain tensor would not have accurately represented the data.

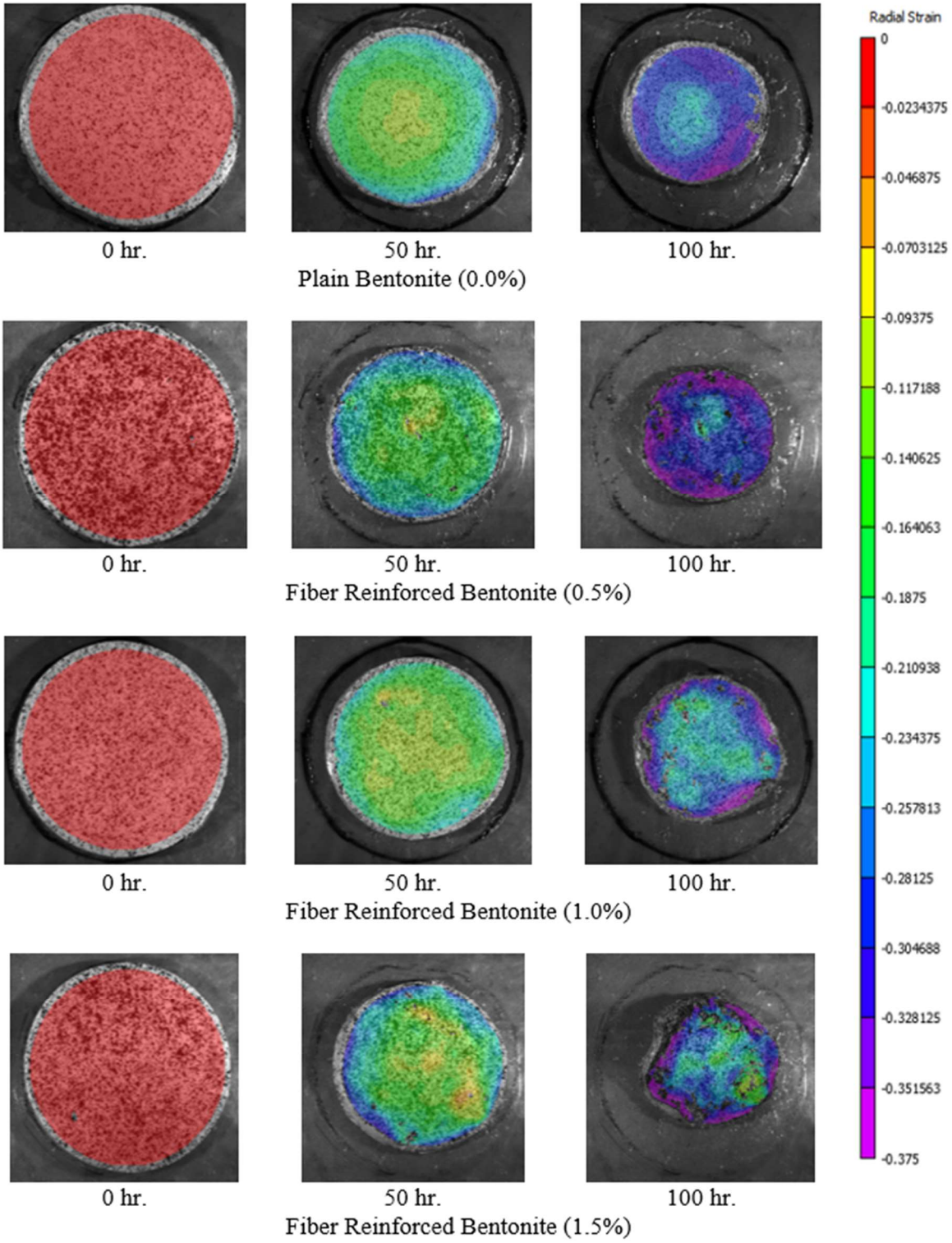

Figure 18. Visualization of radial strain field for free shrinkage disk specimens

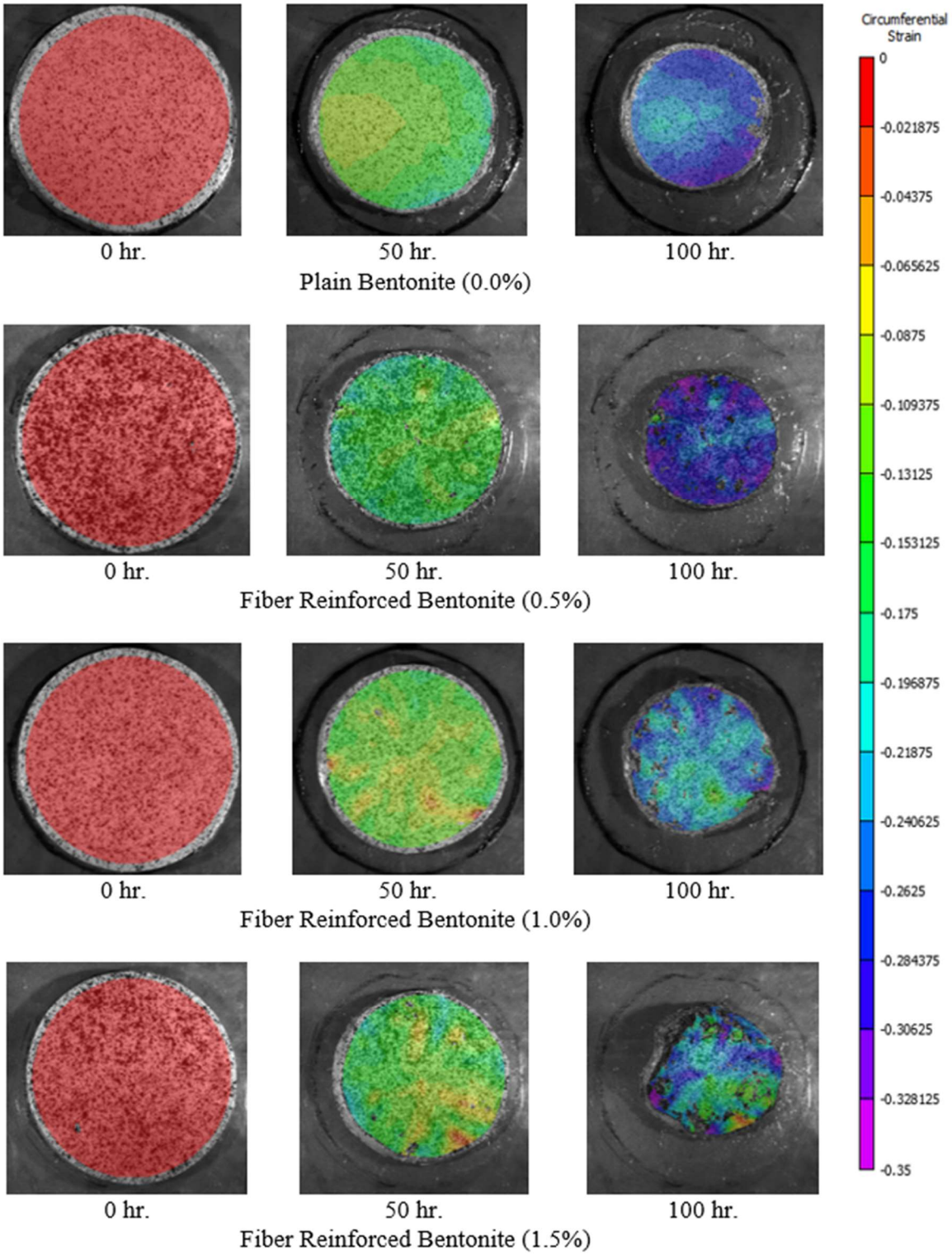

Figure 19. Visualization of hoop strain field for free shrinkage disk specimens

Conclusions

Free shrinkage behavior of plain bentonite clay versus basalt microfiber-reinforced bentonite clay was compared by observing the desiccation of disk specimens for a period of 3-5 days and recording specimen weight and DIC displacements. Only one-dimensional top-surface drying was allowed and fiber contents of 0.0, 0.5, 1.0, and 1.5% by weight were considered. Plain bentonite clay and fiber-reinforced specimens showed similar free shrinkage trend, determined based on specimen moisture loss and diameter reduction trends during testing. However, fiber-reinforcement minimally reduced the rate of free shrinkage. 1.0 % and 1.5 % fiber-reinforced bentonite specimens developed lower radial and hoop displacements and strains, which were successfully determined via DIC analysis. Overall, 1.0 % microfiber-reinforced bentonite showed the lowest shrinkage extent according to all free shrinkage measurements, including lowest rate of diameter decrease, lowest rate of moisture loss, and lowest radial and hoop strains during testing.

CHAPTER IV

DESICCATION CRACKING BEHAVIOR

Introduction

Desiccation cracking testing of restrained-ring specimens with 0.0, 0.5, 1.0, and 1.5% basalt microfiber by weight was conducted for up to 7 days for each replicate. Only one-dimensional top-surface drying was allowed. The specimens experienced a period of free shrinkage for the first 3 days, like the behavior of the free shrinkage disk specimens, with significant reduction in specimen diameter and no crack initiation. Cracking of each specimen initiated from the third day of testing at the soil-ring interface due to the build-up of tensile hoop stresses from the restrained shrinkage condition. The plain bentonite clay and microfiber-reinforced specimens presented clear and distinct desiccation cracking behaviors. Testing was stopped on the seventh day when significant cracking caused loss of contact with the inner restraining ring for the plain bentonite clay specimens. Moisture loss of all specimens was measured indirectly by measuring weight change of specimens during desiccation. Additionally, the evolution of the radial, circumferential, and vertical displacement and strain fields was successfully determined by the DIC method. Note that the results shown in each figure in this chapter represent the average of the results from three or more sample replicates for each basalt microfiber content, except for the radial and hoop strain fields, where a representative sample for each fiber content was chosen. Also note that when the crack width, crack length, radial strain at the crack tip, and hoop strain at the crack tip are examined the crack considered in the analysis is the major critical crack, defined as the

largest (i.e., widest, and longest) crack, which was also generally observed to be the first crack to initiate.

Results and Discussion

Diameter Change

The diameter change, weight change, and moisture profiles were also extracted for restrained-ring specimens. The average diameter change is shown in Figure 20 for the initial stages of testing (i.e., up to 80 hours), when the specimens experienced a period of radial shrinkage before any crack initiation. From the shrinkage period of the restrained ring test, it is again evident that plain bentonite and microfiber-reinforced bentonite experienced similar shrinkage trends, however fiber inclusion reduced shrinkage rate. Shrinkage rate and total extent was again lowest for the 1.0 % fiber case.

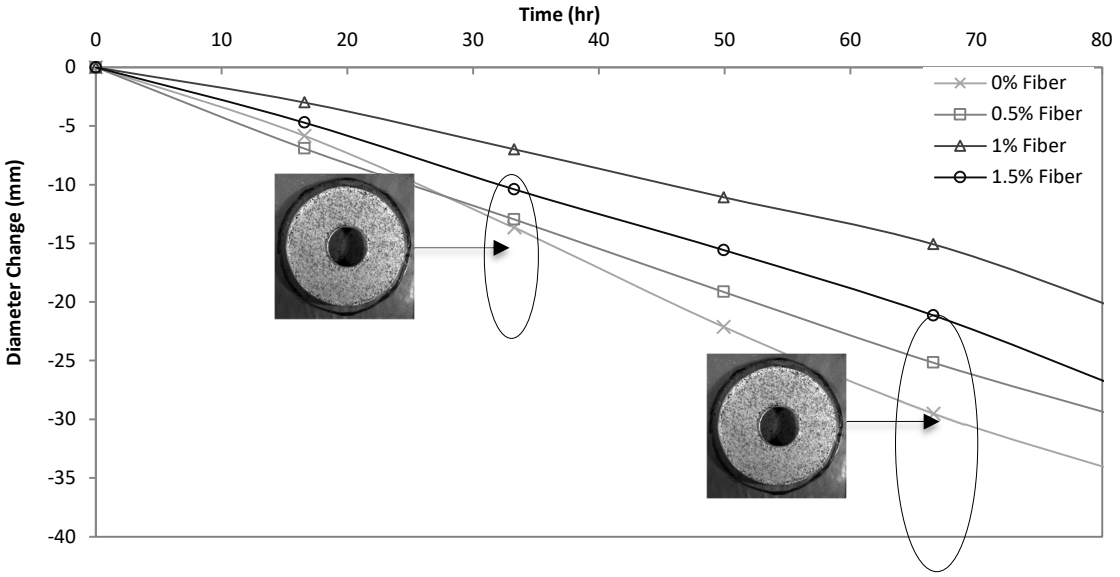

Figure 20. Diameter change of restrained ring specimens

Moisture Loss

The average weight change and moisture loss profiles are shown in Figure 21 and Figure 22, respectively. From the moisture profiles it is also evident that moisture loss trends are similar between the different fiber cases. However, 1.0 % fiber again experienced the lowest rate of moisture loss, which validates its lowest rate of diameter change for the restrained ring test, and its lowest rate of diameter change, moisture loss, and strain development for the free shrinkage test.

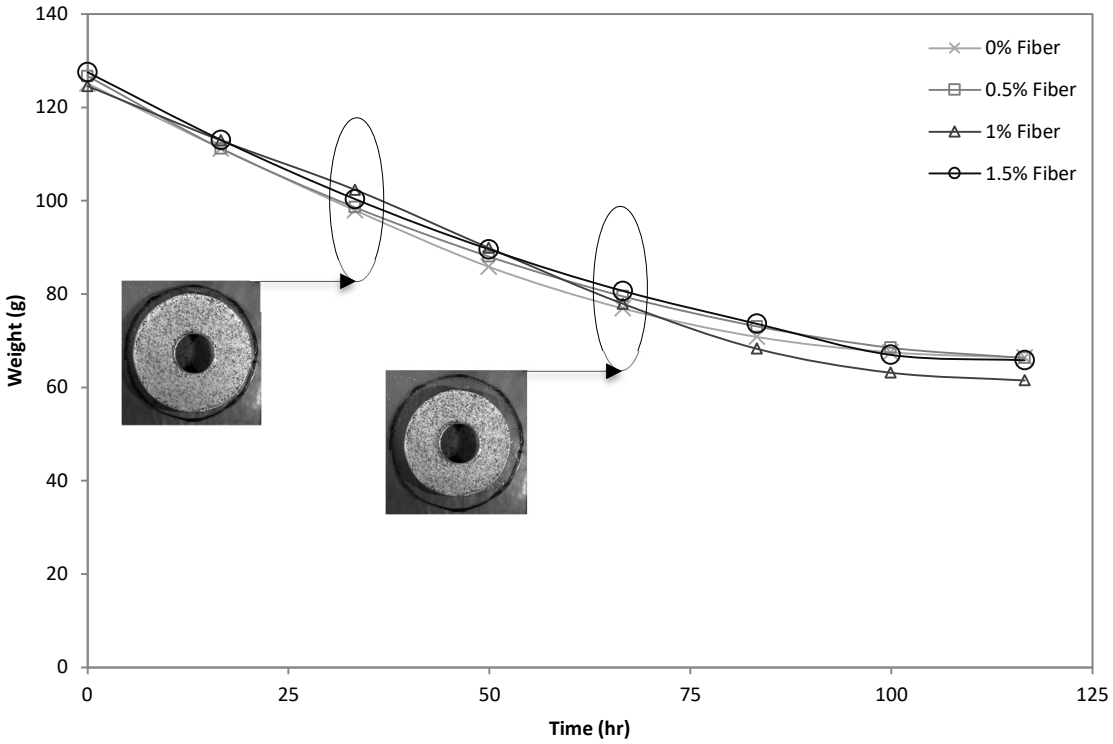

Figure 21. Weight change of restrained ring specimens

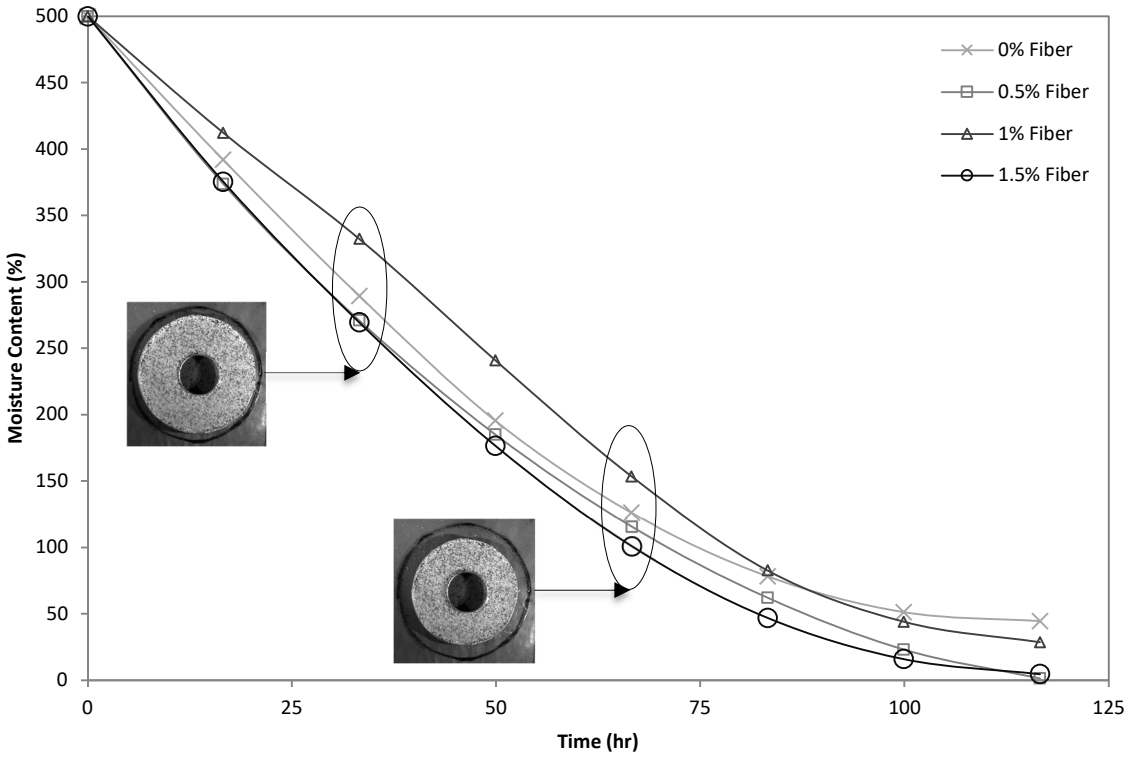

Figure 22. Moisture loss profiles of restrained ring specimens

The lowest free shrinkage rate and extent in the 1.0 % fiber correlated with the maximum out-of-plane deformation or curling and warping effect. The curling and warping occurred during testing because the specimens were only allowed to dry from their top surface, so that over time the top surface of each specimen would shrink and contract. When the surface would shrink and contract, the edges of the sample would easily curl upwards because of the small thickness-to-diameter ratio. This same phenomenon is observed in long thin concrete slabs or sheets of plywood that experience drying shrinkage or temperature gradients.

This upwards deformation or curling was observed to increase with fiber content up to 1.0 % and then decrease for 1.5 % fiber. This curling effect is shown in Figure 23. Both the increase in out-of-plane deformation or sample curling, and decrease in free shrinkage rate and extent with fiber content up to 1.0 %, can be explained by small differences in sample density with moisture content. It was observed that initial sample weights and material density increased with fiber content up to 1.0 % and decreased slightly for 1.5 %, as excess fiber may have re-introduced voids into the material. Thus, since 1.0 % fiber samples had the highest density, they experienced the lowest moisture loss rate leading to the lowest free shrinkage rate and extent. This is because increased density generally leads to decreased void space or smaller refined voids, which decreases hydraulic permeability. The lowest moisture loss can also lead to the largest moisture gradient forming across the thickness of the samples and moisture gradient induces curling behavior. A similar phenomenon has been observed for concrete specimens that have been wet cured, which refines the pore structure of concrete and leads to decreased hydraulic permeability. Similarly, the wet cured samples showed reduced rates of moisture loss, which caused the development of higher moisture gradients and larger curling deformations (Hajibabaee, 2015).

However, since three or more replicates were conducted for each microfiber content, for both the free shrinkage and restrained shrinkage tests, a statistical t-test was conducted to compare the average moisture loss of each microfiber content to the average moisture loss for the plain bentonite case and determine whether the differences in free shrinkage rate and extent with microfiber content are statistically significant. The

moisture content at 70 hours of free shrinkage testing was chosen, as the difference in moisture loss and free shrinkage rate causes notable differences in moisture loss and free shrinkage extent towards the end of testing. Furthermore, 70 hours was the duration of the shortest disk test for any replicate. Thus, the average moisture content could be calculated from the data of three or more replicates for each fiber content. It was hypothesized that microfiber inclusion would decrease moisture loss extent (i.e., increase moisture content at 70 hours) as sample density was increased (with the highest sample density occurring at 1.0 %). Thus, a one-tailed t-test was conducted for each microfiber content, with an alpha value of 0.05 (i.e., 95 % confidence level). The one-tailed p-values obtained were 0.152, 0.158, and 0.196, for 0.5, 1.0, and 1.5 % microfiber content, respectively. Therefore, according to the t-test conducted there is a 15-20% probability that the difference in free shrinkage rate and extent with microfiber content, occurred due to random chance or experimental variation, and an 80-85 % chance that the observed reduction in free shrinkage (as determined by moisture loss) with microfiber addition is 'real'.

Fiber Content: 0.0 % 0.5 % 1.0 % 1.5 %

Figure 23. Visual difference in curling extent for each fiber content

Evolution of Radial and Hoop Strains

The evaluation of radial strains and circumferential (i.e., hoop) strains after 0, 50, and 100 hours of testing, are visualized in **Figure 24** and **Figure 25**, respectively. It can be observed that as fiber content increased the magnitude of the hoop strain field decreased. Thus, the fiber matrix provided tensile resistance to the development of large tensile hoop strains. Fiber inclusion did not have as much effect on the magnitude of radial strains developed.

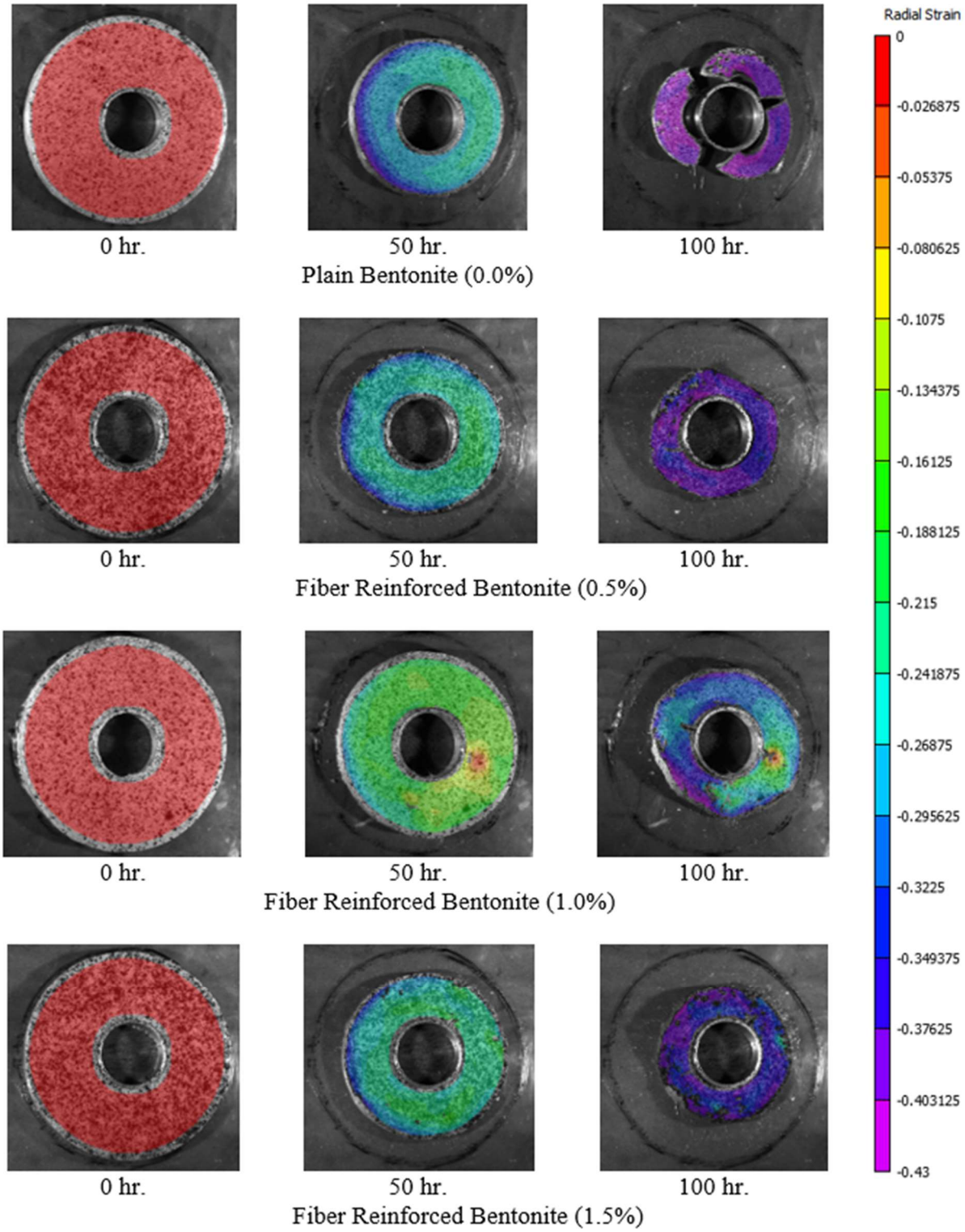

Figure 24. Visualization of radial strain field for restrained ring specimens

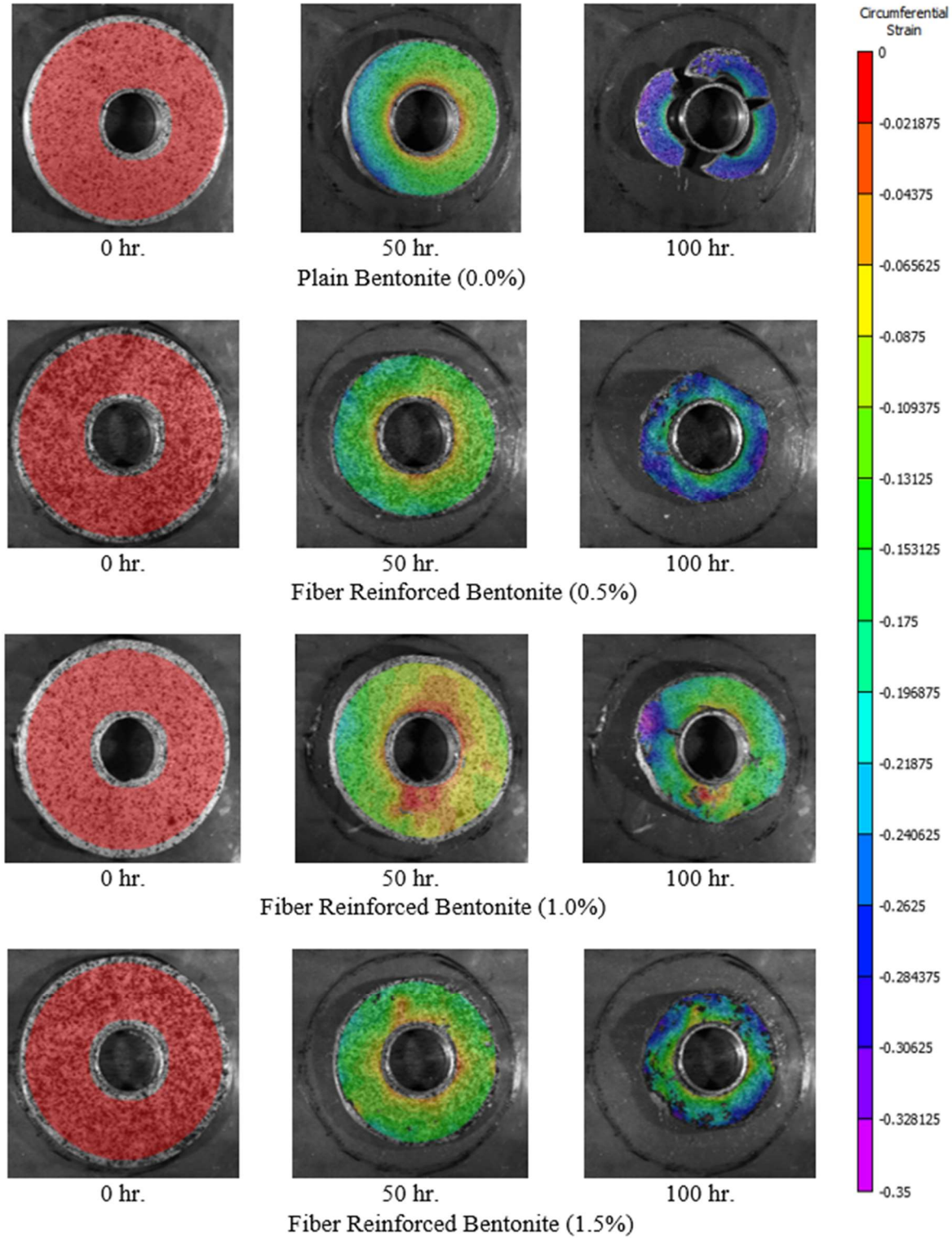

Figure 25. Visualization of hoop strain field for restrained ring specimens

The evolution of radial and hoop strains at the crack tip were also investigated using DIC. Figure 26 and Figure 27 show the radial and hoop strain at the major crack tip, respectively. Basalt microfiber inclusion reduced the development of hoop strains at the crack tip up to 50 % but had minimal effect on the development of radial strains. Note that the strains are shown from the start of testing (i.e., before crack initiation) at 500 % moisture content, until total crack initiation and propagation at the end of testing (i.e., close to 0.0 % moisture content). Radial strains continually increased from the start of testing at 500 % moisture content until the end of testing. However, the hoop strains at the crack tip continually increased from the start of testing and then sharply increased before crack initiation and propagation.

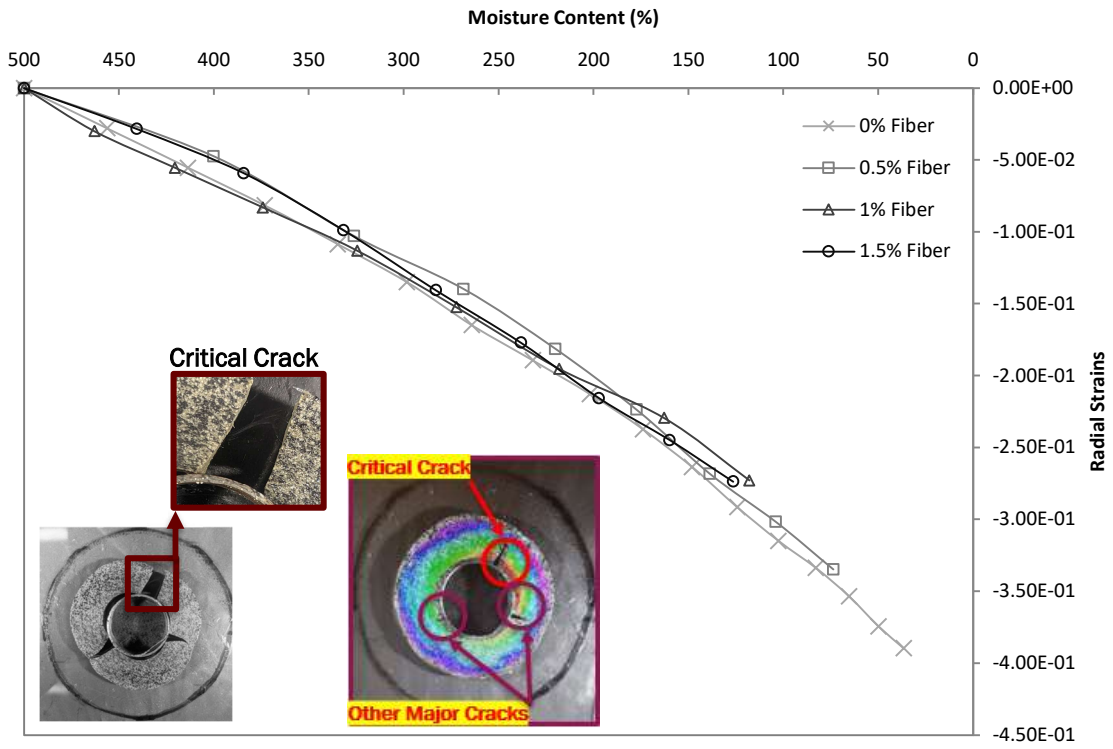

Figure 26. Radial strain at major critical crack tip for restrained ring specimens

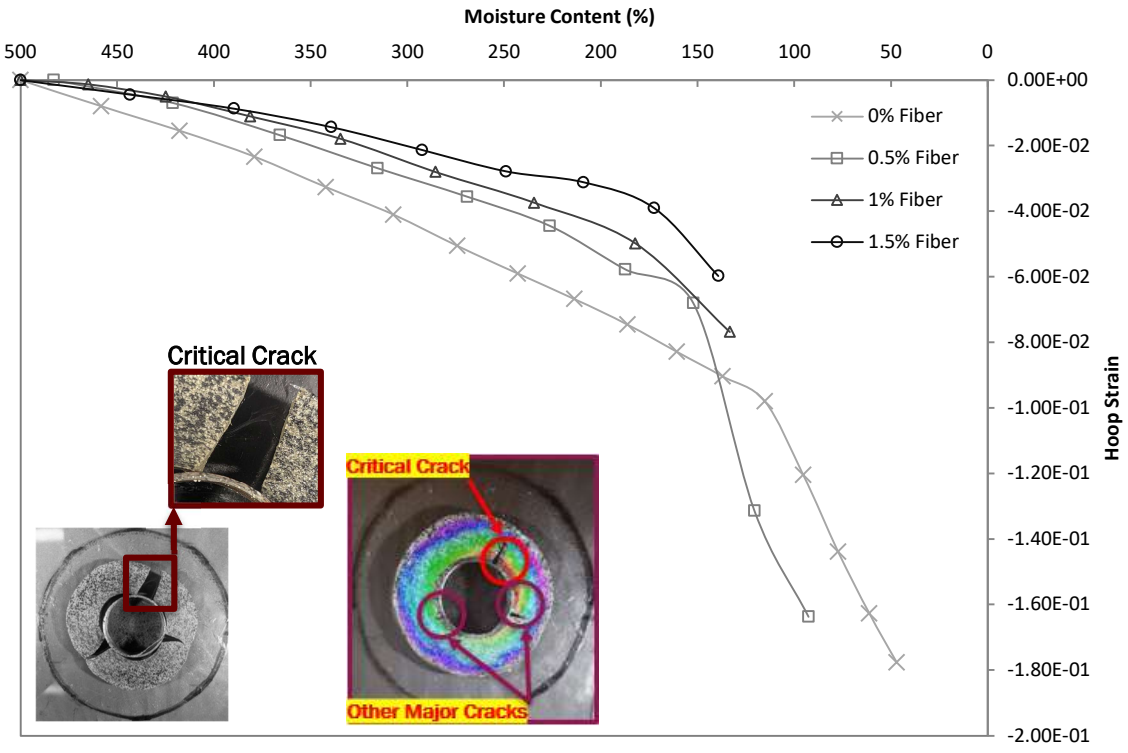

Figure 27. Hoop strain at major critical crack tip for restrained ring specimens

Cracking

The average time and moisture content of crack initiation were recorded for each fiber content and are shown in Table 2. Crack initiation occurred at earlier times and at higher moisture contents as fiber content increased, however the severity of cracking was greatly reduced.

Table 2. Time and moisture content of crack initiation

Fiber Content (%)	0%	0.5%	1%	1.5%
Time (hr.)	83	80	70	40
Moisture Content (%)	87	103	165	227

Figure 28 shows the final crack pattern (i.e., after total crack propagation) from representative samples of each fiber content, after testing. It is evident from the figure that as fiber content increased the crack pattern was changed from three major cracks with complete crack separation to smaller minor cracks that did not fully separate.

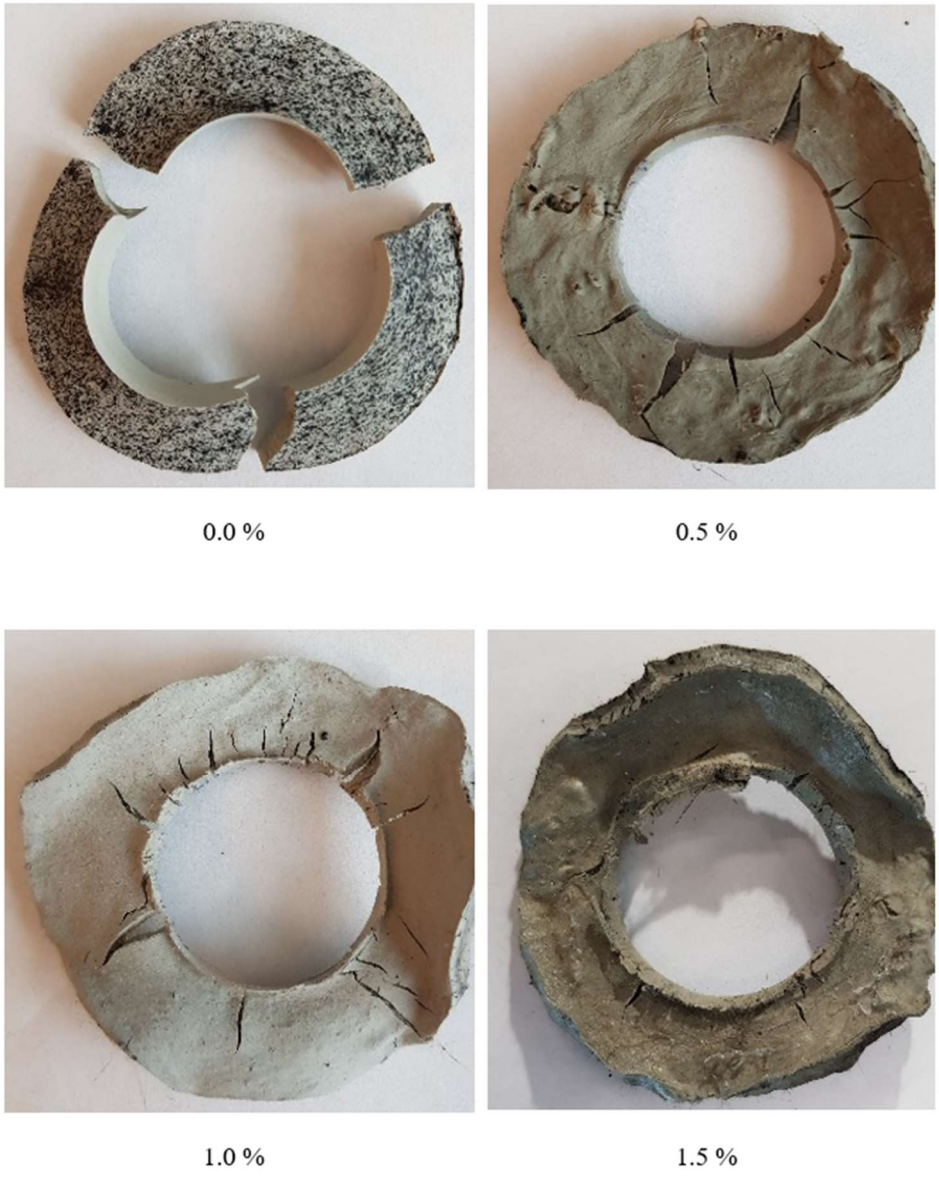

Figure 28. Final crack pattern of restrained ring specimens after testing

For the plain bentonite case each replicate followed this same cracking pattern. Thus, by the end of testing each plain bentonite specimen was divided into approximate thirds by the initiation and propagation of three major cracks, often with one or two cracks initiating first. The complete crack separation caused the plain bentonite specimens to lose contact with the inner restraining ring by the seventh day of testing, hence all desiccation testing was stopped at 7 days. The formation of a few major cracks can still be observed for the 0.5 % and 1.0 % however the crack opening and propagation decreased with fiber content. For the 1.5% fiber case, only small minor cracks clustered around the inner restraining ring can be seen. Table 3 summarizes the differences in cracking behavior and extent between the different fiber contents.

Table 3. Summary of cracking behavior for each fiber content

Fiber %	**Presence of Major Cracks** (yes/no)	**Presence of Minor Cracks** (yes/no)	**Complete Propagation and Separation of Cracking**	**Loss of Contact at Inner Restraining Ring**
0.0 %	Yes (**3 major cracks**)	**No**	**Yes**	**Yes**
0.5 %	Yes (1-3)	Yes (~5-15)	No	No
1.0 %	Yes (1-3)	Yes (~10-20)	No	No
1.5%	**No**	Yes (~15-25)	No	No

The differences in cracking behavior can be explained because the cracks were prevented from widening and propagating by the fiber reinforcement, which resulted in the formation of many minor cracks with earlier crack initiation to exhaust the larger fracture energy. Even after the complete duration of testing (i.e., seven days) none of the basalt microfiber-reinforced specimens experienced complete separation of the material or loss of contact at the soil-ring interface. A closeup view of the basalt microfibers crack-bridging effect is shown in Figure 29.

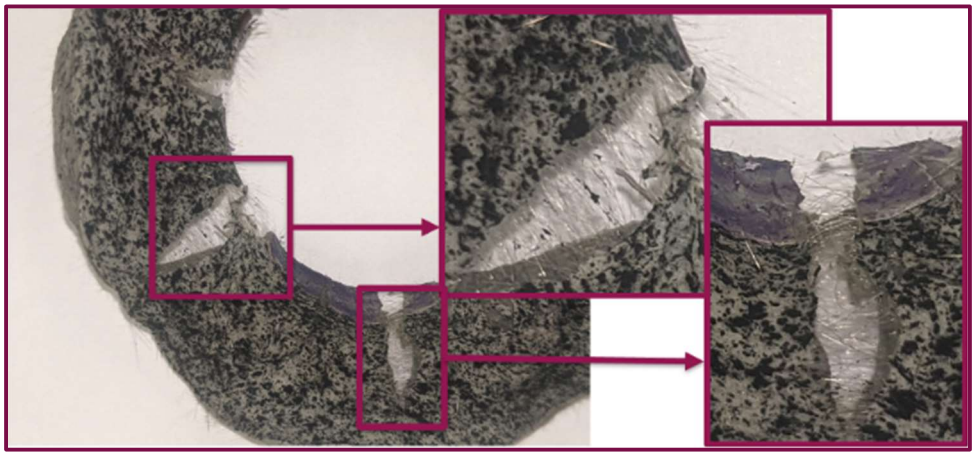

Figure 29. Closeup of "crack-bridging" effect of basalt microfibers

After visual inspection of Figure 28 and Figure 29 it is obvious that the impact of basalt microfibers was to reduce the severity of desiccation cracking for the IMEBM restrained ring specimens compared to the plain bentonite case. To quantify the reduction in crack severity, DIC analysis was used to record the changing distance between two speckle points on opposite sides of the crack mouth during testing. This allowed for a determination of crack width and crack length propagation until crack completion. The evolution of crack width or crack opening displacement is shown in Figure 30. The displacement is shown from the time of crack initiation until the time of

crack completion (i.e., at the end of testing). For the plain bentonite case the crack width continued increasing rapidly until the end of testing. However, for the basalt microfiber-reinforced specimens the crack grew until "fiber-bridging" prevented further opening and crack completion (i.e., no further crack growth) occurred.

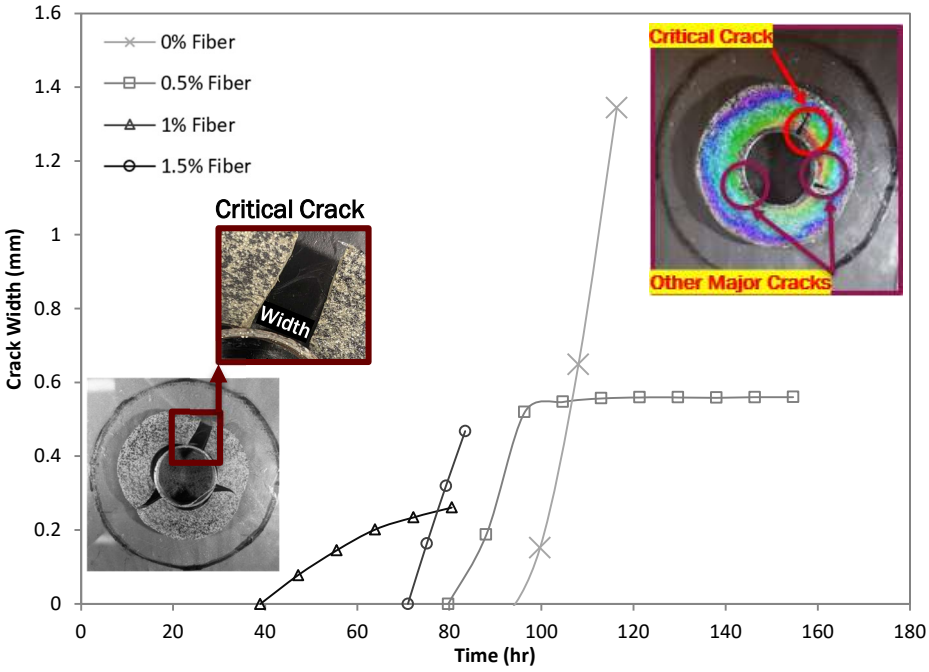

Figure 30. Evolution of major critical crack widening for restrained ring specimens

Thus, the crack width at the end of testing was reduced from 1.34 mm, which was the average crack width recorded at the end of testing for the plain bentonite case, to 0.56-0.26 mm, as crack width decreased with increasing fiber content. That is a 58-76 % reduction in crack mouth opening. A similar trend was observed for crack length propagation, which is shown in Figure 31. Since cracking propagated from the soil-ring interface to the outer edge of the specimen for every plain bentonite replicate, the total crack length can be considered as the entire radius of the specimen (i.e., 35 mm). Like crack width, for the basalt microfiber-reinforced cases crack length grew until the "fiber-

bridging" effect prevented further crack propagation. Crack growth stopped at 13.75, 10.75, and 9.95 mm for 0.5, 1.0, and 1.5 % fiber content, respectively. Thus, fiber inclusion caused a reduction in crack length of 60-72 %.

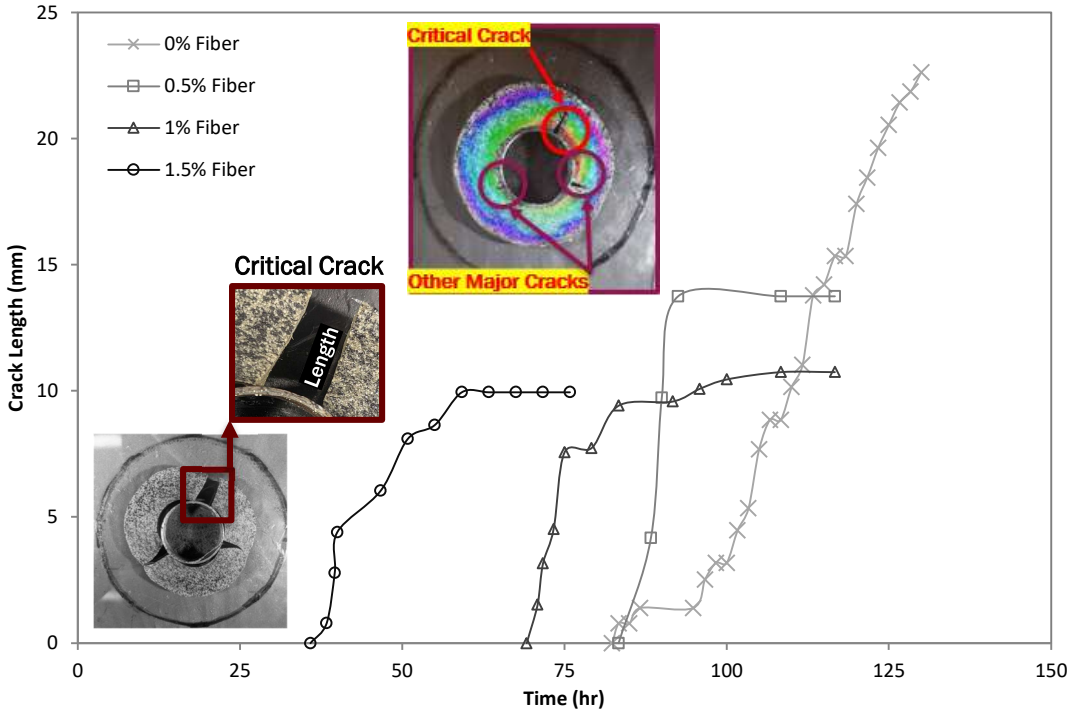

Figure 31. Evolution of major critical crack length propagation for restrained ring specimens

Final major critical crack width and crack length for each microfiber content are tabulated in Table 4.

Table 4. Length and width of major critical crack versus fiber content

Fiber %	Crack Width (mm)	Crack Length (mm)
0.0 %	complete separation (1.34 mm at the end of testing)	through entire sample radius (i.e., 35 mm)
0.5 %	0.56 (**58 % reduction** from **0.0%)**	13.75 **(60% reduction from 0.0%)**
1.0 %	0.47 (**65 % reduction**)	10.75 **(69% reduction)**
1.5%	0.26 (**76 % reduction**)	9.95 **(72% reduction)**

Conclusions

Desiccation cracking behavior of plain bentonite clay versus basalt microfiber-reinforced bentonite clay was compared by observing the desiccation of restrained-ring specimens for a period of 7 days and recording specimen weight and digital image correlation (DIC) displacements. Only one-dimensional top-surface drying was allowed and fiber contents of 0.0, 0.5, 1.0, and 1.5% by weight were considered. The plain bentonite clay and microfiber-reinforced specimens presented clear and distinct desiccation cracking behaviors. Basalt microfiber reinforcement caused cracking to initiate at earlier times and higher moisture contents, however the extent of cracking was dramatically reduced. Plain bentonite specimens developed 3 major cracks that initiated at the soil-ring interface and propagated to the outer edge of the specimen until complete separation of the specimen occurred. However, with increasing fiber content more small minor cracks developed, concentrated around the inner restraining ring. The development of radial and hoop strains around the crack tip was examined and it was

determined that microfiber inclusion does not impact radial strain development and extent. However, hoop strain development was reduced with increasing basalt microfiber content. Microfiber reinforcement was found to be effective in “bridging” any cracks that initiate. Crack length and width were significantly decreased with increasing fiber content. Thus, basalt microfiber reinforcement may be an effective method to prevent and control desiccation cracking in bentonite clay nuclear barriers, to protect public health and safety.

CHAPTER V

CONCLUSIONS

The effectiveness of using basalt microfiber to reduce desiccation cracking in bentonite clay Engineering Barrier Material (EBM) for geological repository of nuclear spent fuel was examined by using the Restrained Ring Test method. Digital Image Correlation (DIC) was used as a noncontact full-field deformation measurement to track the shrinkage and desiccation phenomena and make quantified analysis between plain bentonite and fiber reinforced bentonite with different percentages of basalt microfibers. Based on the analysis the following can be concluded:

1. The DIC method was successful in determining the evolution of radial and hoop displacement and strain fields for both free shrinkage specimens and the restrained ring method.
2. Plain bentonite and basalt microfiber-reinforced specimens showed similar free shrinkage behavior and trends.
3. Basalt microfiber-reinforcement minimally reduced free shrinkage rate. Thus, the radial and circumferential (i.e., hoop) displacements and strains, were decreased by basalt microfiber inclusion.
4. Overall, 1.0 % microfiber-reinforced bentonite showed the lowest shrinkage extent according to all free shrinkage measurements, including lowest rate of diameter decrease, lowest rate of moisture loss, and lowest radial and hoop strains during testing. This was discovered to be due to an increase in initial sample density with microfiber addition up to 1.0 %.

5. Desiccation cracking behavior was significantly influenced by the addition of basalt microfibers.
6. Basalt microfiber inclusion caused cracking to initiate at slightly earlier time and higher moisture contents.
7. Plain bentonite specimens developed three major cracks, which propagated from the soil-ring interface to the outer specimen diameter. However, with increasing fiber contents the specimens developed more small minor cracks concentrated around the inner restraining ring.
8. The radial and hoop strain development around the crack tip was examined. It was found that radial strain development and extent is not influenced by fiber content. However, hoop strain in the vicinity of the crack tip significantly decreased with increasing microfiber content.
9. Microfiber-reinforcement was shown to be effective in "bridging" the cracks, preventing complete crack-tip separation and propagation. Thus, crack length and width were drastically reduced by 58-76 and 60-72 %, respectively. This infers that reinforcing plain bentonite with inorganic basalt microfibers can potentially control desiccation cracking in geological repositories and improve nuclear waste management and safety.

This study is significant as it will contribute to the overall understanding of the mechanisms of desiccation shrinkage and cracking in low permeability clays, specifically the desiccation behavior of bentonite clay, and the impact of microfiber

reinforcement on the trends and extent of shrinkage and cracking. Most notably the proposed research will provide insight on whether fiber reinforcement, particularly basalt microfiber reinforcement, may be an effective solution for controlling desiccation cracking in bentonite clay. This may be useful for various applications where bentonite clay is commonly used and desiccation cracking is an ongoing issue, such as in bentonite clay liners etc. The specific application proposed for this research is to reduce desiccation cracking in bentonite clay used for nuclear waste disposal. Reduction of desiccation cracking in bentonite clay EBM has the potential to significantly prevent increases in hydraulic permeability that may lead to the leakage of toxic contaminants through nuclear waste barriers. Thus, basalt microfiber reinforcement may improve current nuclear waste management practices, for the better protection of public health and safety.

REFERENCES

1. Abdi, M., Arjomand, M., & Parasapajouh, A. (2008). Effects of Random Fiber Inclusion on Consolidation, Hydraulic Conductivity, Swelling, Shrinkage Limit and Desiccation Cracking of Clays. International Journal of Civil Engineering 6(4), 284-292.
2. Akesson, M., Gatabin, C., Jacinto A. C., Ledesma, A., & Sanchez, M. (2009), Bentonite THM Behavior at high temperatures: experimental and numerical analysis, Geotechnique (59), 4, 307-318, https://doi.org/10.1680/geot.2009.59.4.307
3. Alcoverro, J., & Blaheta, R., & Gens, A., & Hasal, M., & Kim, G.-Y., & Kuo, C.-W., & Kuo, W.-J., & Lee, C., & Lee J., & Lin, C.Y., & Michalec, Z., & Takayama, Y. (2021). HM and THM interactions in bentonite engineered barrier materials for nuclear waste disposal. International Journal of Rock Mechanics and Mining Sciences. https://doi.org/10.1016/j.ijrmms.2020.104572
4. Alonso, E., Gens, A., Guimaraes, N., Huertas, F., Lloret, A., Olivella, S., Sanchez, M., & Villar, M. (2009) A full-scale in situ heating test for high-level waste disposal: observations, analysis, and interpretation. Geotechnique (59), 4, 377-399
5. Amarisiri, A., Kodikara, J., & Shannon, B. (2014). Numerical modelling of desiccation cracking in a restrained ring test. Canadian Geotechnical Journal (51), 67-76.

6. Azhari, A., & Isfahani, H.S. Investigating the effect of basalt fiber additive on the performance of clay barriers for radioactive waste disposals. Bull Eng Geol Environ 80, 2461–2472 (2021). https://doi.org/10.1007/s10064-020-02044-x

7. Barton, R., & Ivey, S. (1996). Nelder-Mead Simplex Modifications for Simulation Optimization. Management Science, 42(7), 954-973.

8. Bella, G., Fiore, V., Scalici, T., & Valenza, A. (2015). A review on basalt fibre and its composites. Composites Part B, 74, 74-94. https://doi.org/10.1016/j.compositesb.2014.12.034

9. Biland, A., Chuvashov, Y., Gulik, V., Holiuk, M., Kiisk, M., Kutsyn, P., Kutsyna, I., Odynokin, H., & Romanenko, I. (2019). New composite material based on heavy concrete reinforced by basalt-boron fiber for radioactive waste management. Nuclear Sciences and Technologies, 2(22). https://doi.org/10.1051/epjn/2019050

10. Bouchemella, S., Eid, J., Hajjar, A., Ouahbi T., & Taibi, S. (2019). Desiccation and cracking behaviour of clayey soils: experimental characterization and mechanisms identification. 17th European Conference on Soil Mechanics and Geotechnical Engineering. https://doi.org/10.32075/17ECSMGE-2019-0998

11. Branston, J., Das, S., Kenno, S., & Taylor, C. (2016). Influence of basalt fibers on free and restrained plastic shrinkage. Cement and Concrete

Composites (74), 182-190, http://dx.doi.org/10.1016/j.cemconcomp.2016.10.004

12. Braudeau, E., Mohtar, R., Najm, A. M., & Weiss, J. (2009). Assessing internal stress evolution in unsaturated soils. Water Resources Research, 45, 1-18. https://doi.org/10.1029/2007WR006484

13. Brescia-Norambuena, L., Grasley, Z., Hogancamp, J., & Shi, X. (2020). Fracture Properties and Restrained Shrinkage Cracking Resistance of Cement Mortar Reinforced by Recycled Steel Fiber from Scrap Tires. Journal of the Transportation Research Board, 2674(8). https://doi.org/10.1177/0361198120924407 (2 June 2020).

14. Bulut, R., Chen, L., & Zaman, M. (2020). A study of tensile stress with suction by restrained ring method. Transportation Geotechnics, 23(100306). https://doi.org/10.1016/j.trgeo.2019.100306 (9 December 2019).

15. Chen, Z.-G., Cheng, Q., El-Maarry, M., Shi, B., Tang, C.-S., & Zeng, H. (2020). Tensile behavior of clayey soils during desiccation cracking process Engineering Geology, 279(105909). https://doi.org/10.1016/j.enggeo.2020.105909

16. Cheng, Q., Shi, B., Tang, C.-S., Tian, B.-G., Xu, J.-J., & Zeng, H. (2021). Desiccation cracking of soils: A review of investigation approaches, underlying mechanisms, and influencing factors. Earth-Science Reviews, 216(103586). https://doi.org/10.1016/j.earscirev.2021.103586

17. Costa, S. (2009). Study of Desiccation Cracking and Fracture Properties of Clay Soils [Monash University]. Australia.

18. Costa, S. & Kodikara, J. (2012). Evaluation of J Integral for Clay Soils Using a New Ring Test. Geotechnical Testing Journal, ASTM., 35(6), 1-9. https://doi.org/10.1520/GTJ104271.

19. Cui, Y.-J., Gu, K., Lui, C., Shi, B., & Tang, C.-S. (2012). Desiccation cracking behavior of polypropylene fiber–reinforced clayey soil. Canadian Geotechnical Journal, 49, 1088-1101. https://doi.org/10.1139/t2012-067

20. Cyrus, S. (2008). Studies on the Development and Control of Desiccation Cracks in Compacted Clay Liner Soils [Cochin University of Science and Technology].

21. Czigany, T. & Deak, T. (2019). Chemical Composition and Mechanical Properties of Basalt and Glass Fibers: A Comparison. Textile Research Journal, 79(7), 645-651. https://doi.org/10.1177/0040517508095597

22. D'Ambrosia, M., & Grasley, Z. (2011). Viscoelastic properties and drying stress extracted from concrete ring tests. Cement and Concrete Composites, 33, 171-178. https://doi.org/10.1016/j.cemconcomp.2010.10.014

23. Dhand, V., Hui, D., Mittal, G., Park, S.-J., & Rhee, K. (2015). A short review on basalt fiber reinforced polymer composites. Composites Part B, 73, 166-180. https://doi.org/10.1016/j.compositesb.2014.12.011 (16 November 2014).

24. Dong, X., Duan, W., Hu, S., Xu, Y., Yao, X., Zhang, X., & Zhuang, Y. (2021). The Effects of Fiber Inclusion on the Evolution of Desiccation

Cracking in Soil-Cement. Materials, MDPI., 14(4974). https://doi.org/10.3390/ma14174974

25. Dong, W., Kastiukas, G., Luo, H., Wu, Z. M., & Zhou, X. M. (2018). Quantifying the influence of elliptical ring geometry on the degree of restraint in a ring test. Computers & Structures, 207, 111-120.

26. Eid, S., Hajjar, A. E., Hattab, M., Ouahbi, T., & Taibi, S. (2020). Shrinkage cracking of unsaturated fine soils: New experimental device and measurement techniques. Strain, 56(12352). https://doi.org/10.1111/str.12352

27. Eid, J., Fleureau, J.-M., Hajjar, A. E., Hattab, M., Ouahbi, T., & Taibi, S. (2021). Assessing crack initiation and propagation in flax fiber reinforced clay subjected to desiccation. Construction and Building Materials, 278(122392). https://doi.org/10.1016/j.conbuildmat.2021.122392

28. Gao, L., Inyang, H., Liu, C., Shi, B., & Tang, C.-S. (2011). Experimental Investigation of the Desiccation Cracking Behavior of Soil Layers during Drying. Journal of Materials in Civil Engineering, ASCE., 23(6), 873-878.

29. Gao, C., Liu, K., & Wei, X. (2020). A Review of Cracking Behavior and Mechanism in Clayey Soils Related to Desiccation. Advances in Civil Engineering. https://doi.org/10.1155/2020/8880873

30. Gens, A., Sanchez, M., & Villar M.V. (2008). Behavior of a bentonite barrier in the laboratory: Experimental results up to 8 years and numerical simulation. Physics and Chemistry of the Earth (33), https://doi.org/10.1016/j.pce.2008.10.055

31. Hajibabaee, A., & Ley., T. (2015). The impact of wet curing on curling in concrete caused by drying shrinkage. Materials and Structures (49), 1629-1639

32. Hild, F., & Roux, F. (2006). Digital Image Correlation: from Displacement Measurement to Identification of Elastic Properties – a Review. Strain, 42, 69-80.

33. Hirose, K., & Matsubara, H. (2018). Mechanisms of Mudcrack Formation and Growth in Bentonite Paste. Journal of Geotechnical and Geoenvironmental Engineering, ASCE., 144(4).

34. Kodikara, J., Shannon, B., & Rajeev, P. (2015). The Use of Restrained Ring Test Method for Soil Desiccation Studies. Geotechnical Testing Journal, ASTM., 38(1). https://doi.org/10.1520/GTJ20130131

35. Kouta, N., Saliba, J., & Saiyouri, N. (2020). Effect of flax fibers on early age shrinkage and cracking of earth concrete. Construction and Building Materials, 254, 119315.

36. Leupin, O. X., & Sellin, P. (2013). The use of clay as an engineered barrier in radioactive-waste management–a review. Clays and Clay Minerals, 61(6), 477-498.

37. Ming, H., Tan, Y., & Xu, X. (2022). Analysis of double-layered buffer in high-level waste repository. Annals of Nuclear Energy, 165, 108660.

38. Mohammad, N. (2020). Desiccation Cracking Behavior of Thin Bentonite Layers [The University of Sydney]. Australia.

39. Sampler, J. & Zheng, L. (2008). A coupled THMC model of FEBEX mock-up test. Physics and Chemistry of the Earth (33), https://doi.org/10.1016/j.pce.2008.10.023

40. Shannon, B. (2013). Fracture Propagation of Cohesive Soils Under Tensile Loading and Desiccation [Monash University]. Australia.

41. Soujanya, D., & Thyagaraj, T. (2017). Polypropylene fiber reinforced bentonite for waste containment barriers. Applied Clay Science, 142, 153-162. https://doi.org/10.1016/j.clay.2017.02.009